Pressure Transients within MCS Mesohighs and Wake Lows

JASON C. KNIEVEL AND RICHARD H. JOHNSON

Department of Atmospheric Science, Colorado State University, Fort Collins, Colorado

(Manuscript received 24 June 1997, in final form 7 November 1997)

ABSTRACT

By animating enhanced coarse surface pressure observations of 12 1985 Preliminary Regional Experiment for Storm-Scale Operational Research Meteorology (PRE-STORM) mesoscale convective systems (MCSs) the authors exposed 92 transitory highs and lows living within virtually all of the systems' mesohighs and wake lows. A quasi-Lagrangian (feature following, not material following) analysis of the pressure fields produced five primary results.

First, these transients, with magnitudes of a few millibars, horizontal dimensions of order 100 km, and average lifetimes of about 2 h, collectively composed spatial and temporal envelopes that contributed at least part of the total pressure field within mesohighs and wake lows. Transients did not apparently favor formation or dissipation in any location of the envelopes. Second, as the MCSs matured, the difference between each complex's transitory highs' mean pressure and transitory lows' mean pressure increased in 78% of the conclusive cases. Apparently, one frequent role of MCSs is locally to magnify storm-scale pressure gradients. Third, transient paths reflect the frequent symmetric-to-asymmetric metamorphoses of the MCSs. Fourth, the temporal fluctuations of the numbers and apparent sizes of transients within a composite MCS partially support theories of MCS upscale evolution. Finally, the composite's transient numbers and apparent sizes varied almost identically with time in a pattern that closely resembles the fluctuation of stratiform and convective volumetric rain rates of MCSs.

1. Introduction

Since the 1940s, meteorologists have observed that organized mesoscale convective systems (MCSs) are usually accompanied by some or all of three forms of meso-β (Orlanski 1975) surface pressure perturbations: a presquall low, a mesohigh, and a wake low. This paper concerns the *pressure transients* that compose the latter two. Mesohighs and wake lows appear partly to be spatial and temporal envelopes; for the cases herein, their perimeters circumscribed the collective perimeters of transients within them, and their lifetimes began with the formation of the first transient and ended with the dissipation of the last.

a. Background

Figure 1a is a plan-view schema of an organized (we now drop ''organized'' but imply it henceforth) midlatitude mesoscale convective system (MCS). A convective line of cumulonimbi leads the system. Forward of this line is the presquall low, and collocated or just behind the line is the mesohigh. A band of minimal precipitation, called the transition zone or reflectivity trough, separates the thundershowers of the convective line and the often steady, but not necessarily heavy, rain of the stratiform region (Ligda 1956; Sommeria and Testud 1984; Chong et al. 1987; Smull and Houze 1987b; Johnson and Hamilton 1988; Zhang and Gao 1989; Biggerstaff and Houze 1991; Braun and Houze 1994). The wake low is at the back edge of the stratiform anvil.

During about the past half century, this leading line–trailing stratiform combination gradually has emerged as a common precipitation motif among organized MCSs (Williams 1948; Newton 1950; Pedgley 1962; Zipser 1969, 1977; Houze et al. 1990). However, observed systems often deviate from this idealized archetype. In the westerlies that are typical of the Great Plains, the most vigorous cumulonimbi may favor the southern part of the convective line (Newton and Fankhauser 1964; Skamarock et al. 1994; Scott and Rutledge 1995), resulting in a sickle or comma pattern (Fig. 1b). Not all MCSs contain a distinct transition zone or stratiform region. When the mean vertical wind shear vector parallels the convective line instead of crossing it front-to-rear (FTR), little or no anvil and little or no stratiform rain develop (Heymsfield and Schotz 1985). Very strong upper-tropospheric rear-to-front (RTF) winds may spread the stratiform anvil ahead of the leading cumulonimbi instead of behind them (Newton 1966; Houze and Rappaport 1984; Roux 1988). Even when stratiform regions do trail their parent eastbound storms,

Corresponding author address: Jason C. Knievel, Department of Atmospheric Science, Colorado State University, Fort Collins, CO 80523-1371.
E-mail: knievel@hook.atmos.colostate.edu

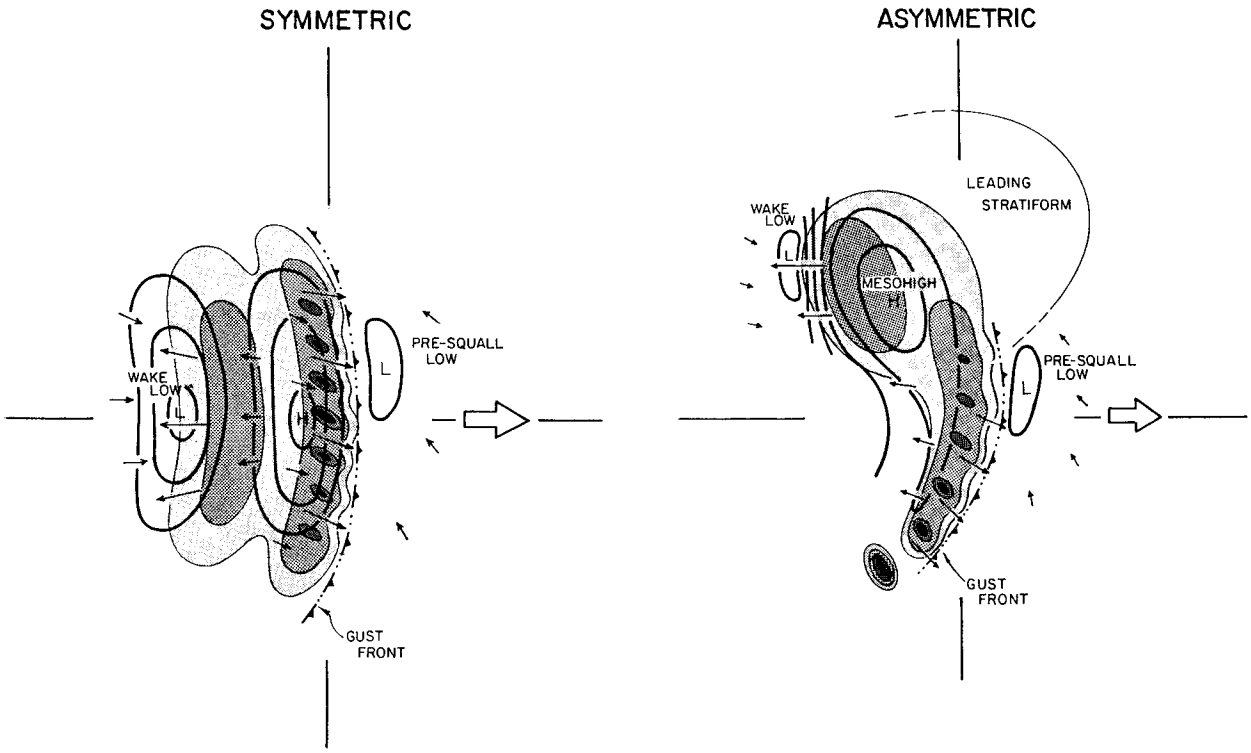

FIG. 1. Schemata of the symmetric and asymmetric stages of an MCS. Shading represents radar reflectivities adapted from Houze et al. (1990); intensity increases with darkness. Solid curves are isobars at every millibar. Small arrows depict the surface winds; arrow length indicates speed. Storm motion is left to right [from Loehrer and Johnson (1995)].

often the anvil and its precipitation are more intense or expansive, not directly to the west, but to the northwest or southwest (Newton 1950; Pedgley 1962; Ogura and Liou 1980; Srivastava et al. 1986; Schmidt and Cotton 1989; Houze et al. 1990; Skamarock et al. 1994; Loehrer and Johnson 1995).

When the stratiform region trails directly behind the convective line so the centroids of the two are collinear with their mutual motion vector (Fig. 1), a system is called symmetric (Houze et al. 1990). In systems that are asymmetric, the stratiform region favors the left or right side of the convective line—usually the left in the Northern Hemisphere.

Until recently most studies were one snapshot, or a small group of snapshots, of an MCS. Meteorologists documented a brief excerpt from the life of some midlatitude system, and in their glimpse they would find a symmetric MCS (Ogura and Liou 1980; Srivastava et al. 1986; Smull and Houze 1987a,b) or an asymmetric MCS (Brunk 1949; Newton 1950; Pedgley 1962; Schmidt and Cotton 1989), or maybe an MCS that was not, or could not be, put into either category (Kessinger et al. 1987; Houze et al. 1990). Not until field research programs such as Preliminary Regional Experiment for Storm-Scale Operational Research Meteorology (PRESTORM) made more comprehensive, continual MCS observations possible did researchers discover that the symmetric and asymmetric patterns that sometimes appear are not two *types* of MCSs, but two *stages* of some MCSs (Skamarock et al. 1994; Loehrer and Johnson 1995; Scott and Rutledge 1995). That is, regardless of initial convective structure, many midlatitude MCSs tend toward asymmetry late in life.

Considerable evidence suggests that the precipitation and wind fields of an MCS shape the system's surface pressure field. Mesohighs are produced by saturated downdrafts that raise pressure hydrostatically because of the atmosphere's response to cooling by evaporation, sublimation, and melting (Humphreys 1929; Suckstorff 1935; Sawyer 1946; Byers and Braham 1949; Fujita 1959), and because of water loading from the added mass of rain and ice within downdrafts (Shaw and Dines 1905; Sanders and Emanuel 1977; Nicholls et al. 1988). Dynamic pressure rises as downdrafts strike the ground (Suckstorff 1939; Bleeker and Andre 1950; Fujita 1963, 1985; Wakimoto 1982). Mesohighs advance with an MCS's leading convective line, the source for these three mechanisms. Since the work of Byers and Braham (1949) meteorologists have known that thunderstorm mesohighs compose the overall mesohigh beneath the convective line, but researchers have not determined the statistical properties of the smaller perturbations.

Wake low formation is more obscure. Persuasive studies indicate that rain and snow evaporatively and sublimatively cool midtropospheric RTF flow and render it more dense than its immediate surroundings (neg-

TABLE 1. Twelve subject PRE-STORM MCSs. Column 1 contains the MCS dates; N and S signify the northern and southern MCSs of 13 May. Column 2 contains the transient observation intervals. Column 3 lists proximate synoptic and mesoscale features: southerly 850-mb jet (J), stationary front (SF), cold front (CF), surface pressure trough (T), dryline (DL), and outflow boundary (OB). Column 4 lists the velocities (in degrees from north) of the leading edges of the convective lines (Loehrer 1992). In column 5, Type 1 MCSs grew from disorganization into asymmetric systems with small convective lines in the south and stratiform rain in the north. Type 2 MCSs were at first linear, then their northern stratiform regions developed. Type 3 MCSs back-built as their southwestern gust fronts converged with the ambient flow; old convection in the north turned stratiform. In Type 4 MCSs, east–west and northeast–southwest convective lines intersected, enhanced stratiform rain developed northwest of the apex, then the east–west line died. Type 5 MCSs did not turn asymmetric within the PRE-STORM array. Italicized numbers mark MCSs that began as symmetric then became asymmetric.

Date	Observation interval (UTC)	Synoptics	Velocity (m s^{-1})	Type
7 May	0600/07 to 1250/07	J SF	19.2 from 287°	4
13 May (N)	1225/13 to 1945/13	J CF	20.0 from 213°	5
13 May (S)	1505/13 to 1845/13	J CF	16.2 from 275°	2
27 May	0510/27 to 0830/27	J T DL OB	17.5 from 280°	*3*
28 May	0900/28 to 1520/28	SF	18.3 from 300°	*3*
3 June	1510/03 to 1845/03	SF	18.5 from 260°	1
3–4 June	2120/03 to 0230/04	SF	18.6 from 250°	4
4 June	0735/04 to 1225/04	J SF	19.0 from 246°	1
10–11 June	2235/10 to 0750/11	CF T OB	15.6 from 308°	*2*
15 June	0150/15 to 0950/15	J CF	12.1 from 338°	5
24 June	0045/24 to 0820/24	J SF DL OB	10.0 from 350°	2
26–27 June	2005/26 to 0615/27	J CF	08.6 from 316°	5

atively buoyant) (Braham 1952; Atlas et al. 1969; Stensrud et al. 1991; Gallus and Johnson 1995a). The newly created mesoscale downdraft accelerates, and once its accompanying precipitation is diminished or gone, the draft's adiabatic warming prevails (Braham 1952; Krumm 1954; Pedgley 1962). Horizontal and vertical inertia drives downdraft air toward the ground even though it eventually becomes warmer and less dense than the adjacent atmosphere (positively buoyant), so it decelerates (Fujita 1963). Divergence above the resultant pocket of warm boundary layer air reduces the integrated atmospheric mass (Humphreys 1929; Brown 1963; Williams 1963; Riehl 1968; Zipser 1969, 1977; Johnson and Hamilton 1988; Zhang and Gao 1989; Stumpf et al. 1991). Sometimes downdrafts reduce the depth of surface cold pools and thereby lower surface pressure even though the drafts do not descend completely to the surface. This mechanism contributed one-third of the surface pressure falls in the 3–4 June MCS (Stumpf et al. 1991). These processes generally occur within the descending rear inflow jet of an MCS (Smull and Houze 1987b), thereby placing the surface wake low(s) at the rear edge of the stratiform rain (Johnson and Hamilton 1988). In the modeled MCSs of Gallus (1996) and of Wicker and Skamarock (1996), intense surface pressure gradients formed beneath descending rear inflow that impinged on *collapsing* pockets of precipitation.

Because wake lows travel far behind the towering cumulonimbi of the convective line, Brunk (1953) speculated that thunderhead tops might excite gravity waves along the tropopause when they strike it and that wake lows are a surface response to the waves. More contemporary investigators have shown that convective systems do, in fact, generate gravity waves (Bosart and Cussen 1973; Schubert et al. 1980; Koch et al. 1988), and such waves appear to be at least partly responsible for the mesoscale kinematics within MCSs (Pandya and Durran 1996), but their exact contribution to the perturbed surface high and low pressure fields beneath MCSs is still somewhat mysterious.

b. Motivation and objective

Data from the PRE-STORM network afford a rare opportunity to explore detailed observations of the surface fields perturbed beneath MCSs. The signals hidden within these data are clues to the atmospheric clockwork that drives such storm systems because surface pressure characteristics reveal the vertically integrated effects of the dynamical and microphysical character of MCSs. Other studies have intimated that mesohighs and wake lows harbor smaller features (Byers and Braham 1949; Brunk 1953; Williams 1953; Fujita 1955; Pedgley 1962; Johnson and Hamilton 1988; Wicker and Skamarock 1996), and such features are occasionally mentioned in passing, but observations of them heretofore have not been scrutinized. Because reliable observation is the ultimate touchstone against which scientists judge theory, no speculation about how MCSs perturb the pressure fields beneath them can be validated without scrutinizing the smaller features within mesohighs and wake lows. In addition, we cannot gauge the realism of a modeled MCS pressure field without knowing the real field itself.

From PRE-STORM surface pressures recorded during passages of 12 MCSs (Table 1), we translated temporally fine data into spatially fine data, animated the resultant fields, and made quasi-Lagrangian [feature following, not material following (Bluestein 1992)] traces of the revealed transients. This allows us to address four specific issues: 1) the temporal changes in the strengths

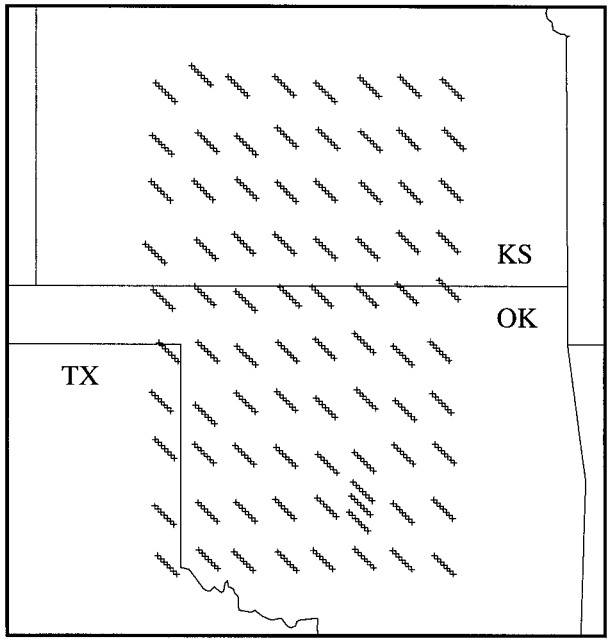

FIG. 2. Data distribution after time–space enhancement; each "+" marks the location of a datum. Data are arranged in clumps of seven and the middle "+" of each seven marks the location of a PAM II or SAM site. Clumps are separated by roughly 50 km.

of transitory highs and lows, 2) transient paths and 3) changes in kinematic scales as MCSs mature, and 4) relationships among transient numbers, transient sizes, and MCS rain rates. There is a less tangible but more profound fifth issue, too: *Perhaps meteorologists' current mental models of mesohighs and wake lows have been spectrally filtered by coarse observations that fail to capture meso-β pressure perturbations' true smallness and brevity*. Moreover, it is likely that additional smaller, more short-lived pressure phenomena exist within the discovered transients, but they escaped detection within the limited scale of the PRE-STORM array, despite the employed time-to-space translation.

2. Data

An overview of the mission and operational program for the 1985 Oklahoma–Kansas PRE-STORM is available from Cunning (1986). Instrument characteristics for the PAM II stations can be found in Johnson and Toth (1986).

a. Surface observations

In situ instruments for PRE-STORM included 42 National Center for Atmospheric Research (NCAR) second-generation Portable Automated Mesonet (PAM II) stations and 42 National Severe Storms Laboratory (NSSL) Surface Automated Mesonet (SAM) stations deployed in a quasi-regular grid with roughly 50 km between sites (Fig. 2). Each station measured dry- and wet-bulb temperatures, station pressure, 5-min averages of wind speed and direction, peak wind over those 5 min, and accumulated rainfall.

We manipulated station pressure data in three ways. First, we negated the influence of station elevation by normalizing the station pressures to 480 m (the average PRE-STORM station elevation) following the example of Loehrer and Johnson (1995). Second, we filtered out pressure oscillations produced by the diurnal solar tide (Chapman and Lindzen 1970; Johnson and Hamilton 1988; Stumpf 1988; Loehrer and Johnson 1995). Third, we removed systematic station-specific biases by using the corrections provided by Loehrer (1992) in appendix A of his paper. Loehrer determined his corrections based on altitude-adjusted station pressures from nearby National Weather Service (NWS) surface synoptic stations according to the method described by Fujita (1963) and Johnson and Toth (1986).

By their very nature, surface pressure perturbations are a measure of processes through the depth of the atmosphere, not simply of lower- and midtropospheric properties. For this reason we found that fields of potential temperature and equivalent potential temperature, which were measured at the surface, were too poorly correlated with surface pressure to greatly aid in locating transients.

b. Radar

We used plots of 0.5° plan position indicator (PPI) reflectivity composites from NWS WSR-57s located at Amarillo, Texas; Oklahoma City and Norman, Oklahoma; Wichita and Garden City, Kansas; and Monett, Missouri. The NWS second-generation radar data processor (RADAP-II) digitized most of the data. The exceptions were at Wichita, where investigators used the Hurricane Research Division NOAA/ERL/AOML digitizer, and in one case at Norman, where they used the NOAA/ERL/NSSL digitizer.

3. Methods of analysis

Three analysis techniques enhanced the PRE-STORM 50-km spatial resolution, maximized detected pressure gradients, and reduced the influence of data voids between stations.

a. Creating space from time

We assumed that the 12 subject MCSs were in steady state for 0.5-h intervals as they moved across the PRE-STORM array (Yang and Houze 1996). This allowed us to relocate a pressure observed at time t a distance $n\Delta t|\overline{\mathbf{u}}|$ up- or downstream, then assign that pressure to that new location at time $t - n\Delta t$, where $n = 3, 2, 1, 0, -1, -2, -3$; $\Delta t = 5$ min; and $\overline{\mathbf{u}}$ is average velocity of an MCS's leading convective line (Fujita 1955; Pedgley 1962).

b. Objective analysis

We objectively analyzed these enhanced data using the iterative weighted-average interpolation scheme developed by Barnes (1964). The scheme assigns to a grid datum a value based on surrounding raw data that fall within a radius of influence (ROI). The contributions of these surrounding data are weighted according to their proximity to the grid datum, and the weighting function is

$$\eta = \exp\left(\frac{-r^2E}{R^2}\right),$$

where r is the distance between the grid datum being calculated and each contributing raw datum, and R is the ROI. Further, E describes how many e-folds in weighting occur for raw data one ROI away from a grid datum. We set E to 4, which ensured that raw data exactly at the ROI (where $r = R$) were weighted by e^{-4}, or 0.018. The sharp decrease of weight with distance insulated the highly localized gradients inherent in convective and mesoscale phenomena from smoothing by more broadscale fields. We varied the ROI from 55 to 165 km so that a minimum of seven reliable data contributed to each objectively analyzed point. The variable ROI mitigated the Barnes scheme's occasional poor treatment of irregularly spaced data. It allowed us to tune the weighting to a value ideal for the finely spaced data, which yielded highly resolved pressure fields, yet it prevented missing data from causing voids in the analyses. We iterated the interpolation scheme three times.

c. Contour maps and movies

From the objectively analyzed data we constructed, using cubic splines under tension, surface pressure plots isoplethed every half millibar, which necessarily smoothed our data one additional time.

Theoretically, the time–space translation forces transients to exist for at least 0.5 h. Some did not. The fault lies with the employed NCAR graphics isoplething routine. We included transients younger than 0.5 h only if their observed lifetimes were abbreviated because they ventured beyond sight of the PRE-STORM array.

Animations of surface pressure plots proved invaluable to our search for MCS transients. Lingering false signals that eluded initial quality control (see section 2) stood unmistakably fixed at station sites amid the fluid signature of the evolving pressure field. We ignored these fixed signals and all other signals produced by any uncorroborated lone PAM II or SAM station. Transients that crossed the domain of inoperative stations often disappeared for a time, only to reemerge as seemingly different perturbations when reliable stations detected them farther downstream. We compensated for the blind spots in the array by projecting highs' and lows' paths across the voids until the transients reemerged.

d. Correlation with radar reflectivity

We included as transients only highs under or near convection and only postsquall lows under or near any part of the reflectivity field, convective or stratiform. Attempts to associate each transient with a corresponding unique stratiform or convective rain core proved fruitless because of gaps in radar data, but we recommend exploration of such connections.

e. Gravity waves

Gravity waves are probably one of the vehicles for the tropospheric mass redistribution within MCSs that necessarily link latent heating and cooling with low and high pressure perturbations. Indeed, gravity wave theory provides an objective framework for a quantitative analysis of the interrelationships among temperature, pressure, and wind. However, a rigorous application of gravity wave theory to these data deserves a separate research effort and far exceeds the scope and available length of this paper. Recognizing gravity waves' probable involvement, we did not attempt to remove their signal from our surface pressure data, although we did restrict our study to pressure transients closely associated with the MCS precipitation fields.

4. A test of analysis accuracy

To test our analyses' accuracy, we hand drew a fictitious but representative MCS pressure field (Fig. 3), then mimicked an MCS's trek across the Great Plains by sliding, with a scale velocity of 16 m s^{-1} from 315°, the drawn field across a map of the PRE-STORM array. We passed the resultant fabricated observations through the objective analysis and through the NCAR graphics isoplething, which produced Fig. 4.

The input and output fields resemble one another quite closely. Both contain four transients—three highs and one low. Additionally, the analysis resolved the two lobes of presquall low pressure and the local low in the northern part of Fig. 3. The true magnitudes of the local extrema did not completely survive the process, but the differences are only a few tenths of a millibar. Most importantly, *the analysis did not introduce any false transients or conceal any real ones.* Other tests proved that the strengths, sizes, and numbers of depicted transients were reasonably insensitive to variations in MCS speed and direction within our analysis routine.

5. PRE-STORM transients

The 12 subject MCSs produced 92 transients—53 highs and 39 lows—that were directly associated with the systems' postsquall precipitation fields. The transitory highs occurred within or just to the rear of the leading convective line, and the transitory lows were predominately at the back edge of, and less frequently

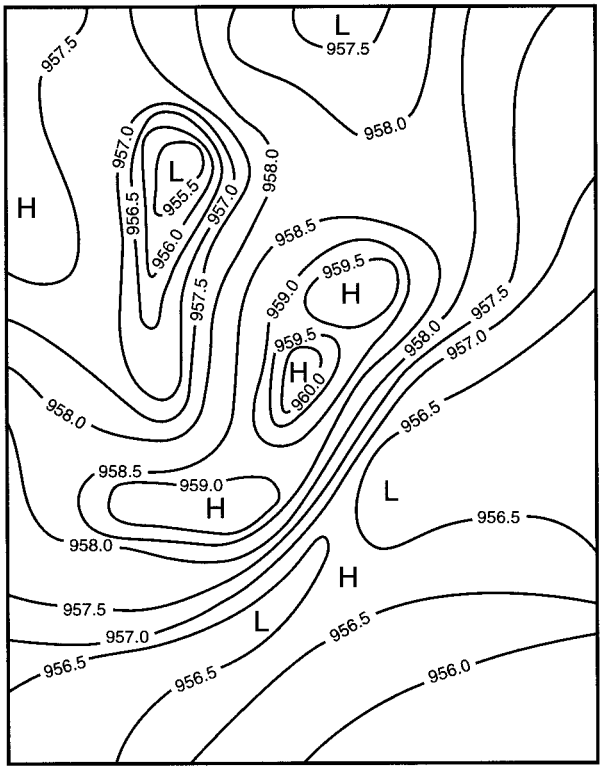

FIG. 3. Test pressure field for analysis verification. Solid lines are isobars at half-millibar intervals. We submitted to our three-step data processing this contrived pressure field. The resultant analyzed field appears in Fig. 4.

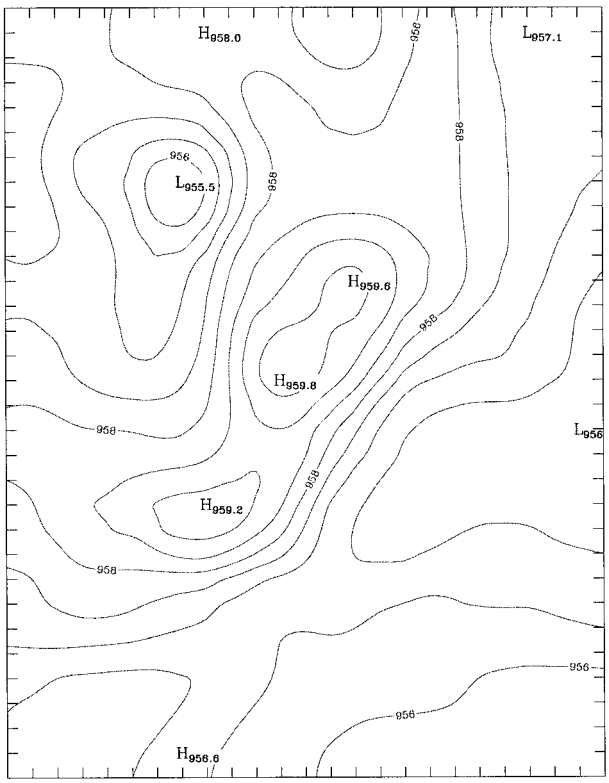

FIG. 4. Verification pressure field. Solid lines are isobars at half-millibar intervals. Three steps of data processing produced this field from the submitted field shown in Fig. 3.

within, the stratiform region. Figure 5 is a representative pressure plot, with schematic radar reflectivity superposed on it. Most of the local pressure extrema in Fig. 5—indeed, most of the extrema in the hundreds of other pressure analyses not shown—were eliminated from the transient population by the above methods, which illustrates the perils of placing much faith in individual images. (The schematic depiction of radar reflectivity in Fig. 5 is only in the interest of visual clarity; we used raw PPI plots in our analyses.)

The 92 transients occurred in families whose members we judged to be closely associated with one another 1) if they were close together and separated by extremely high pressure gradients, 2) if a group of high and low transients moved in similar patterns and remained close to each other during their lives, or 3) if the transients were produced by a division of a preceding transient. Occasionally the distinction between families was ambiguous, but bookkeeping demanded a decision even if it was arbitrary.

The first letter of a transient's name signifies its pressure perturbation: H for high, L for low. The second letter is a transient's family name. The third character, a number, is assigned to avoid ambiguity; these numbers are sequential from 1 through 9. A family usually (but not always) contains both transitory highs and transitory lows. For instance HA2 and LA1 belong to the same family because their mutual proximity implies an association. Notice that the third character, the number, does not imply a special subfamily association among transients with like numbers. For example, HB2 and LB2 belong to the same family, but that is the extent of the link. Although members of different families were not necessarily physically isolated from each other, links across families were distinctly less apparent than links within families.

Most of the 92 transients presented one persistent dilemma. Their centers were clear and precisely located (to the limit of our objective analysis), but their edges were not, especially when transients abutted one another. Determining individual sizes was often impossible as the edge of one bled into the edge of another. Even so, the perimeter of transients' total footprints (the envelopes) were almost always apparent. Because individual transients' centers were more well defined than their edges, we surveyed two center-specific properties: lifetimes and displacements.

a. Detectable lifetimes

A detectable lifetime is the difference between the times a transient was first and last observed. Only 38 of 92 (41%) transients spent their complete lives within

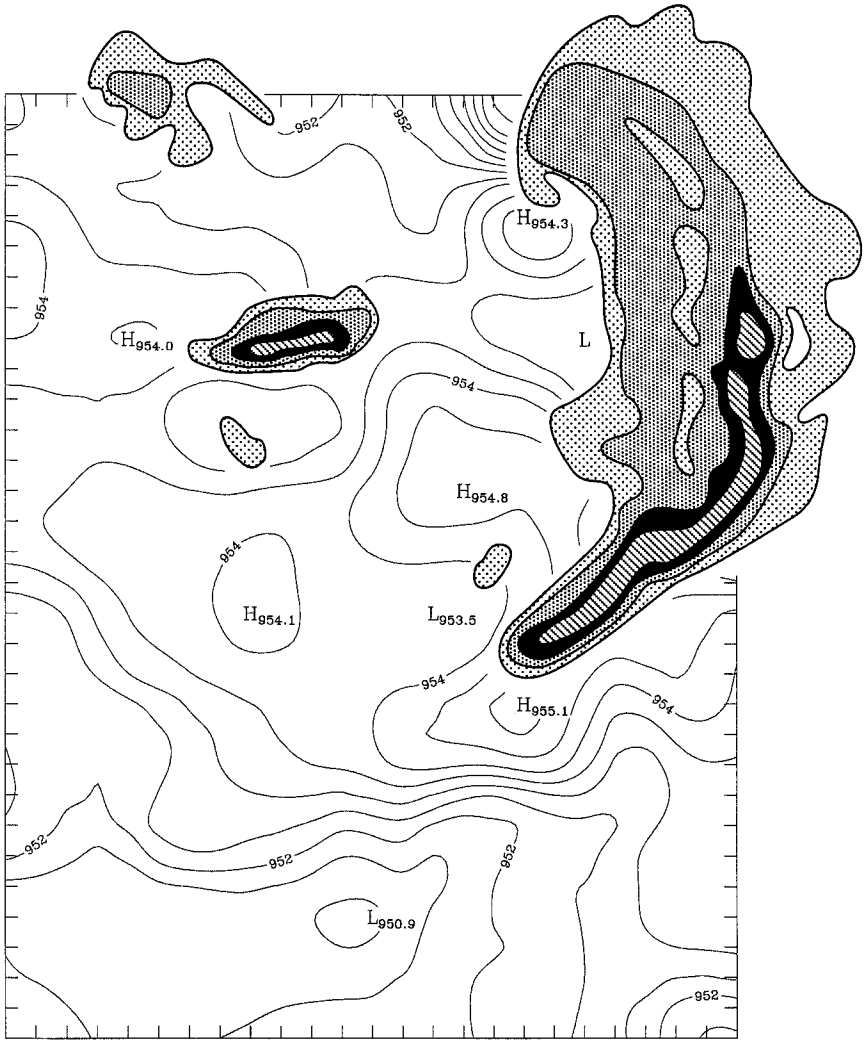

FIG. 5. Station pressure (mb) and schematic radar reflectivity (shaded zones of 15–24, 25–39, 40–49, and 50–64 dBZ) for 1400 UTC 28 May 1985.

the PRE-STORM array. These 38 do not represent the overall transient population because long-lived, well-traveled transients are more likely to escape complete sampling. If the faster MCSs had produced more short-lived transients the bias would be mitigated, but there is no evidence of such a tendency (Fig. 6). In fact, the data suggest a positive correlation between transient lifetime and MCS speed, but the data are too few to warrant a definite conclusion.

Figure 7 comprises histograms of transient sampled lifetimes. Neither lows nor highs have a clearly preferred longevity (although a weak maximum appears between 1 and 1.5 h), and both populations have sampled lifetimes that range from roughly a 0.5 h to almost 5 h. The average transitory high lifetime for the total population is 124 min (much longer than the lifetimes of individual thunderstorm cells) and the average for all transitory lows is 116 min (Figs. 7a,b). Most of the populations existed less than 3 h.

Excluding the partially sampled transitory lows markedly shifts that population to lower values (Fig. 7d), again because the briefest transients were more likely to spend their comparatively short lives within the limited PRE-STORM instrument ranges. The population of highs also changes with the exclusion (Fig. 7c), but less drastically. Transitory highs with roughly 1-h sampled lifetimes now lead the population, although comparatively many of the 3–4.5-h highs survived the cut. More than 0.5 h separates the average fully sampled lifetimes of the transitory highs and lows. The difference implies that either the local dynamical and thermodynamical perturbations responsible for forming lows did not persist as long as those that produced highs, or that the storm environment modified cold pools more slowly than it changed processes above the surface that contributed to wake lows.

Both Figs. 7c and 7d are loosely bimodal. Transients with lifetimes of less than 2 h account for at least half

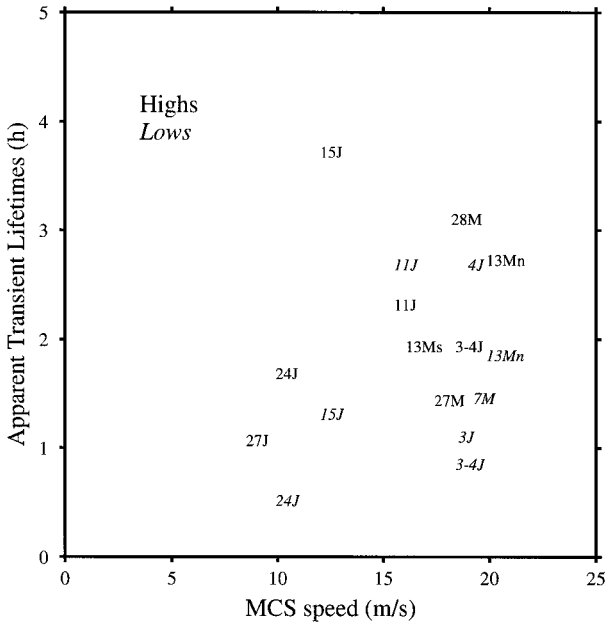

FIG. 6. Average MCS transient lifetime vs leading-line speed. Data are for fully sampled transients only.

of each respective population, but both highs and lows have secondary maxima at the long-lived ends of their histograms, highs in the 3.5–4.5-h bins and lows in the 2.5–3.5-h bins. The fully sampled 23 highs and 15 lows are statistically small populations, so assignment of a physical explanation to the bimodality would be presumptuous.

b. Detectable displacements

Detectable displacements are the observed *net* distances the transients traveled, *not* the total distances. As in the previous section, the first two histograms (Figs. 8a and 8b) depict all 92 transients, while only the fully sampled transients contribute the data for the second two (Figs. 8c and 8d). Transitory highs were not well traveled. Most of them moved less than 150 km before dissipating. When the population is limited to fully captured highs, the reduced group retains the same character as the larger (compare Figs. 8a and 8c).

Well-traveled transitory lows were even rarer than well-traveled highs, which is consistent with their shorter average sampled lifetime. Less than one-sixth of the lows dissipated more than 150 km from their origin.

Generally, the sampled displacements of highs slightly exceed those of lows. A possible explanation is that as an MCS stratiform region blossomed, the rear edge of the anvil expanded relatively rearward, so it moved forward more slowly than the convective line (Houze 1993). Transitory highs, driven predominately by convective cells, advanced with the MCS leading edge. However, mesoscale lows, which were apparently associated with stratiform rain, slowed (see section 1).

c. Quasi-Lagrangian traces

A quasi-Lagrangian analysis (Bluestein 1992) was necessary to expose the fleet, ephemeral transients. Figures 9a–l document the temporal changes in the central pressures of the 92 transients with the diurnal solar tidal effects removed (see section 2a). Each plot comprises two groups of generally horizontal traces. Highs are in the upper group, lows in the lower.

The traces fluctuate on four scales. On the broadest scale, each plot exhibits a mean slope of all the lines. This is some combination of the synoptic and meso-α (or MCS-scale) pressure tendencies; this is the large-scale signature. On the second scale, the means of each group of high traces and each group of low traces show the surface pressure forcing by the convective line and the stratiform region. Although the difference in the two means is not strictly the mesoscale pressure gradient induced by an MCS—this would require the distances between perturbations—consider it a proxy for the gradient. The third scale is the families and includes both highs and lows. They reveal any lag between the time of strongest highs and the time of strongest lows, or vice versa. On the finest scale are the individual transient traces.

Short vertical lines abut one or both ends of some traces. A vertical line at the start of a trace marks a developed transient's emergence into the array and a vertical line at the finish of a trace marks an active transient's disappearance beyond the array edge.

Large-scale pressure rose in 5 (42%) cases, fell in 1 (8%) case, and did not change significantly in 3 (25%) cases; 3 (25%) cases are inconclusive. Pressure trends of transitory highs and lows are collectively diffluent (that is, the central pressures of transitory highs increased while the central pressures of transitory lows decreased) in 7 of 12 (58%) MCSs: 7 May, 13 May (S), 28 May, 3 June, 3–4 June, 4 June, and 10–11 June. Plots of 13 May (N), 27 May, and 26–27 June are inconclusive. The only nondiffluent trends are for the 15 and 24 June storms. As mentioned, pressure trend diffluence is not synonymous with an increase in pressure gradient, but the two are loosely comparable because, for each MCS, the distance between the overall high and low pressure envelopes varied within consistent limits. In this light, it appears that one of the frequent (but not requisite) roles of MCS is to magnify storm-scale pressure gradients, which then presumably slowly diffuse through fluxes and mixing after an MCS departs or spends itself.

Some transitory lows clearly lagged in initiation and strength the highs within the same family (e.g., family C of 28 May and family A of 10–11 June), but such obvious signatures are too infrequent to support conclusions about whether, as a rule, meso-β lows lag meso-β highs within MCSs, and whether such intrafamily lags have preferred durations. Even so, the larger-scale mesohighs and the transients they harbored generally pre-

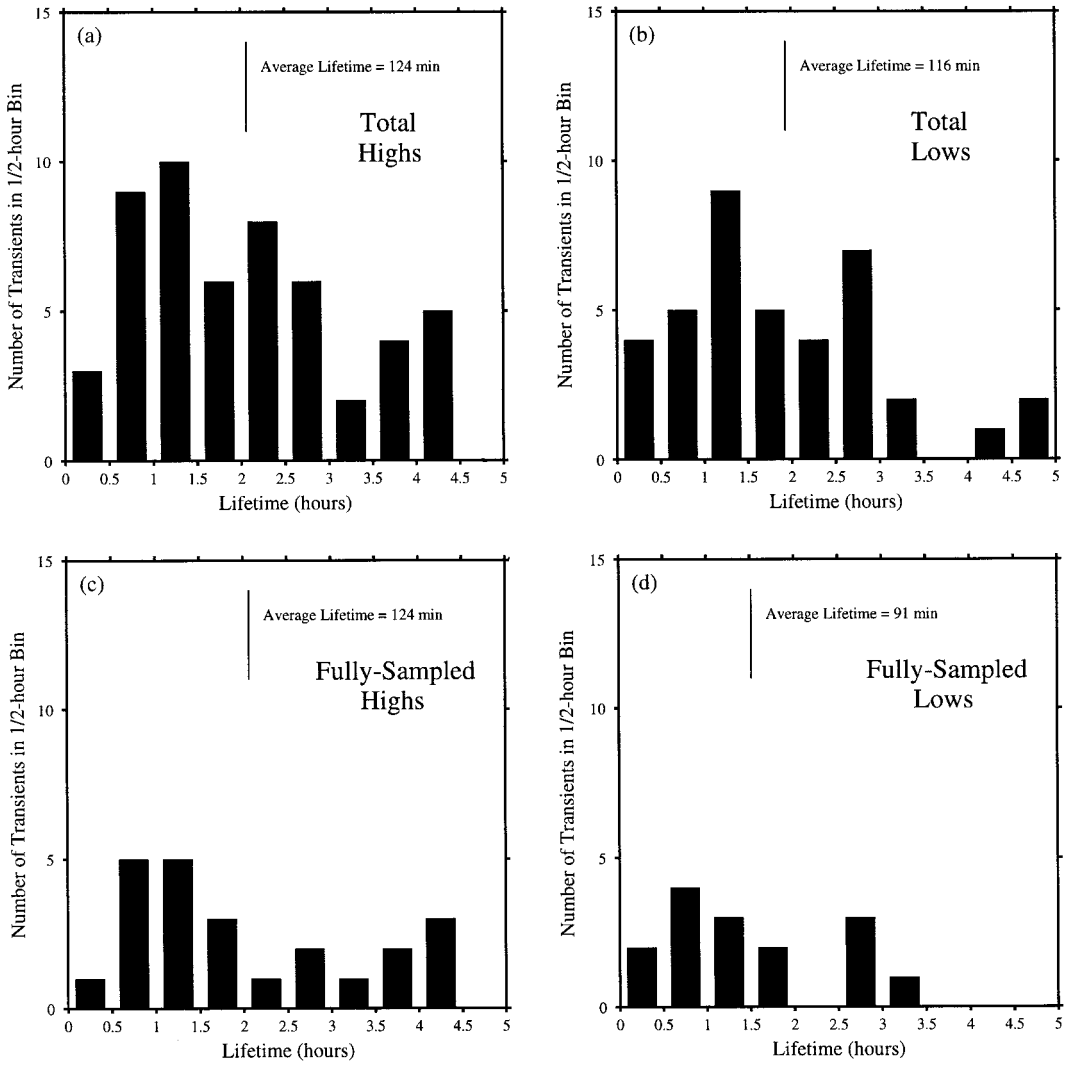

FIG. 7. Histograms of transient lifetimes: (a) total transitory high lifetimes, (b) total transitory low lifetimes, (c) fully sampled transitory high lifetimes, and (d) fully sampled transitory low lifetimes. Fully sampled transients are those that spent their complete lives within the PRE-STORM array.

ceded the larger-scale wake lows and their transients, as depicted by Fujita (1963).

6. Transient paths and MCS symmetry

As MCSs grow beyond their first stages of organization, the three fundamental precipitation regions within most systems—the convective line, the stratiform region, and the transition zone between them—often shift positions with respect to one another. The paths of the 92 surface pressure transients reflect these shifts.

For ease of understanding, consider the illustrated transient paths (Fig. 10) to be variations on two archetypal patterns: parallel and skew. Most families did not exhibit purely one pattern or the other, but if we overlook the ragged tracks produced by the coarse 25×32 Barnes grid (see section 3) most routes taken by the highs and lows are predominately parallel or predominately skew. The paths in Fig. 10 are family-specific only for viewing clarity; although definitions of parallel and skew may be considered from an intrafamily perspective, the two categories may be considered from an interfamily/intra-MCS perspective too. The latter is probably more relevant because MCS leading line–trailing stratiform arrangements are storm-scale, and the latter is probably safer because this perspective obviates doubt about placement of transients within families. Each figure shows an *accumulation* of transient paths, so not all the transitory highs and lows depicted in Fig. 10 existed at the same time.

a. Intrafamily paths

The first family of the first case produced a good example of a pair of parallel transient paths (Fig. 10a).

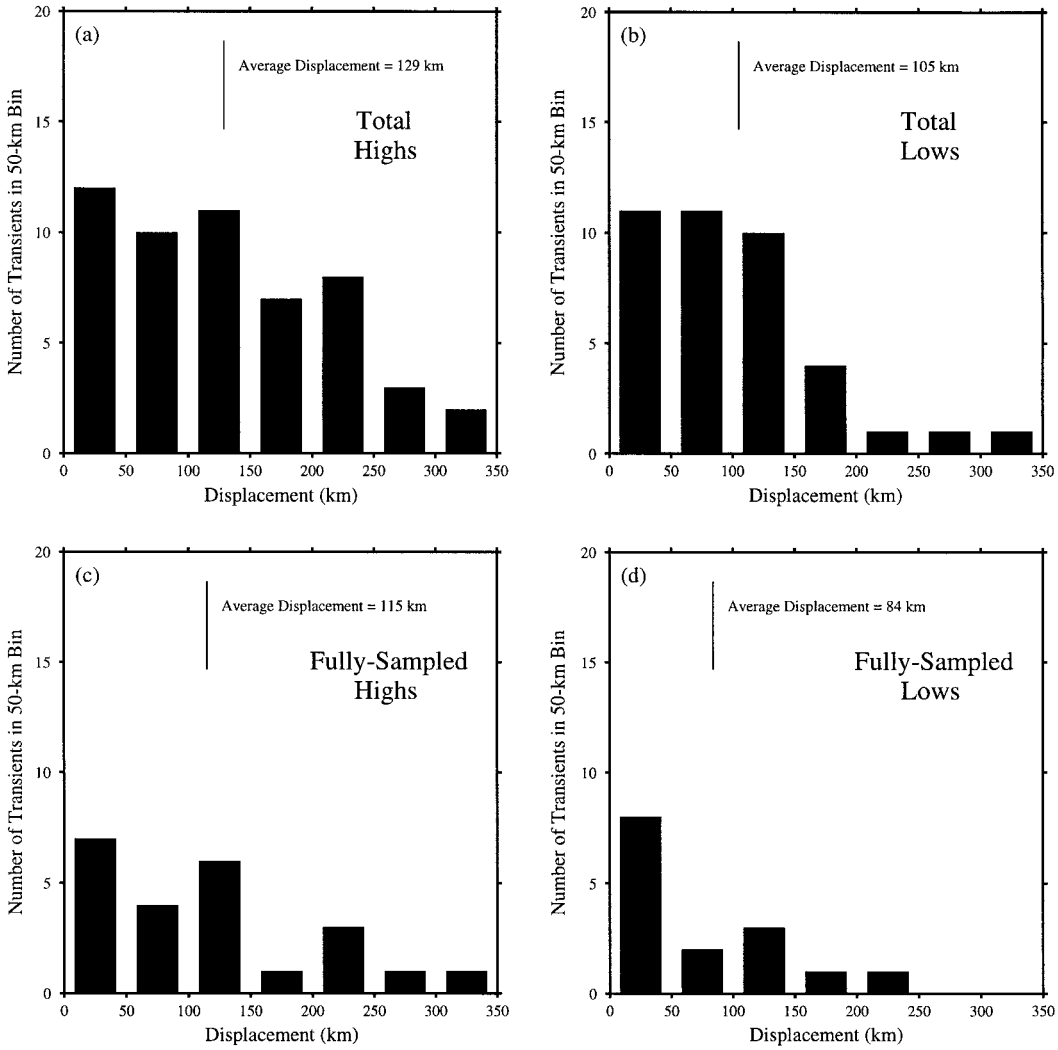

FIG. 8. Histograms of transient displacements: (a) total transitory high displacements, (b) total transitory low displacements, (c) fully sampled transitory high displacements, and (d) fully sampled transitory low displacements. Fully sampled transients are those that spent their complete lives within the PRE-STORM array. Displacements are the *net* distances the transients traveled, *not* the total distances traveled.

(The grid-level raggedness is an artifact.) HA1 and LA1 together moved generally southeastward. Not all parallel paths are as straightforward. HC1 and HC2 of 13 May (N) traveled quasi-parallel to one another (Fig. 10c), for although their paths meander, the angle between their *mean* direction vectors is negligibly small.

Family C of 28 May is an archetypal skew family (Fig. 10d). HC1 formed in the north-central part of the array and moved southeastward. LC1 formed south of HA1's origin and moved straight eastward. Their motion vectors form an angle of roughly 45°.

In many cases transients traveled in a manner that combined characteristics of parallel *and* skew paths. Sometimes initially skew paths turned parallel, as in the cases of family B of 3 June (Fig. 10e) and 15 June's family D (Fig. 10g), while other times parallel paths became skew, as in the case of family A of 24 June (Fig. 10h). Family B of 10–11 June exhibits both changes (Fig. 10f).

Other families' transients maintained consistent courses, but both parallel and skew sets of paths occurred. The northern of the 13 May MCSs produced five family B transients (Fig. 10b). HB1 and LB1 traveled to the northeast, while HB2, LB2, and LB3 followed a more north-northeasterly route. Paths of HB1 and LB1 are parallel, and paths of HB2, LB2, and LB3 are parallel, but the paths within the first group are not parallel to the paths of the second group (e.g., the paths of LB1 and LB3 are skew).

b. Interfamily paths

A simultaneous examination of all of the transient paths of each MCS provides insight into how transients

repositioned themselves relative to one another in cases where the parent system turned asymmetric (Houze et al. 1990; Loehrer and Johnson 1995). Studies have shown that surface pressure perturbations' arrangements imitate the asymmetry of radar reflectivity regions (Fig. 1).

Note that even a single pair of high and low perturbations may be considered either symmetrical or asymmetrical. In the former case, a high and low are collinear with an MCS's motion vector, and in the latter case a low perturbation lies to the left or to the right of an MCS motion vector that is drawn through the leading high.

Both parallel and skew paths are possible vehicles for asymmetrical rearrangement. Skew paths' role is easily guessed: a high–low pair originally aligned one behind the other will change its orientation if the low travels at some angle to the left of the high's direction of travel (Pedgley 1962). That is generally what happened on 28 May (Fig. 11). At 1025 UTC, HA1, HB1, and LB1 were arranged only slightly asymmetrically. Highs' southeastward and lows' eastward advances exaggerated asymmetry during the nearly 3.5 h that followed. At 1200 UTC, HA1 had moved far southeast and was joined by HC1, while in the north HB1 had dissipated. LB1 continued steadily to the east. At 1345 UTC the persistent northern transitory low, LB1, had been joined by LC1, while much farther southeast HC1 was the lone transitory high; HA1 was gone. The skew pattern does not imply that every transient that exists early in a system's life will still exist at the end of its life. New transitory highs and lows formed to replace those that dissipated, and these newly generated transients perhaps formed right or left of the old ones, which itself contributed to a system's symmetry or asymmetry, supplementing or opposing the skew paths' role.

This very substitution of asymmetrically located transients for symmetrically located transients is how MCSs produced an increasingly asymmetric pressure field *even when transients traveled parallel to one another*. The initial symmetrically arranged transitory highs and lows dissipated, then subsequent highs formed to the right of old highs and/or new lows formed to the left of old lows. Observe the 4 June MCS (Fig. 12). All transient paths were parallel. The system was rooted in disorganization so it is not classified as a symmetric MCS in its early stages, yet its early transient arrangement was quasi-symmetric. At 0830 UTC, HA1 and HB1 were staggered north-northeast/south-southwest, and behind them to the west were LA1 and LB1. By 1000 UTC, HA1 had traveled ahead of the other transients and dissipated, leaving HB1, LA1, LB1, and a new low, LB2, which formed to the left of HB1, the lone high at the time. The 1000 UTC pattern was almost exactly symmetric, yet only 1 h later the final two transients, HC1 and LB2, were positioned asymmetrically. During that intervening hour, LB1 and LA1 dissipated and, more importantly, HB1 dissipated and was replaced far to the right (east) by HC1; LB2 maintained its path. The loss of the rightmost low, LB1, the loss of the leftmost high, HA1, and the gain of the rightmost high, HC1, were paramount to the eventual asymmetric last stages of transient arrangement in the 4 June MCS.

The 28 May and 4 June storms are archetypes of the two path classes. Transient paths of the other 10 MCSs are more confused and fall somewhere between these two limits. The two path patterns are useful conceptual tools for visualizing what may happen to transients in the life of an increasingly asymmetric MCS. The patterns may also be clues to the restructuring of the kinematics and latent energy exchanges that may asymmetrize some midlatitude MCSs, because transients' formation, travel, and dissipation are a reflection of the storms' internal structures.

7. Temporal changes in transient number and collective perimeter

Figures 13 and 14 depict a composite of the 12 MCSs. (The appendix explains the compositing method.) The increase and decrease in the number of transients within the composite, and the collapse and expansion of the perimeters of transient footprints are two clues to the role convective and stratiform rain play in generating the transients, and are clues to the evolution of kinematic scales within MCSs.

a. Transient number versus time

The variation in average number of total transients (Fig. 13) is nearly symmetric about the apparent midpoint in the composite system's life because the two curves of the transitory highs and lows, although individually asymmetric, are nearly exact mirror images of each other reflected about scaled time 1/2. The average number of highs peaked about one-third of the way through the composite's observed life, then steadily decreased to nearly 0 at its life's end. Few lows (ignoring presquall lows) appeared early in the composite's observed life, then they increased in number, if a little unsteadily, and reached a maximum at about scaled time 2/3. They then became fewer, but did not quite reach 0, through the end of the observed life. These findings are consistent with the idea that the convective line, which generates thunderstorm downdrafts and mesohighs, comes first in the life of squall lines and the trailing stratiform region, with which wake lows are closely associated, follows (Fujita 1963).

b. Transient perimeter versus time

The three curves in Fig. 14 document the collective transient perimeter (a proxy for area) of the composite system. Figure 14 resembles Fig. 13 remarkably, almost eerily, closely. It is smoother, which is explained in the appendix, but the plots are elementally identical. Note

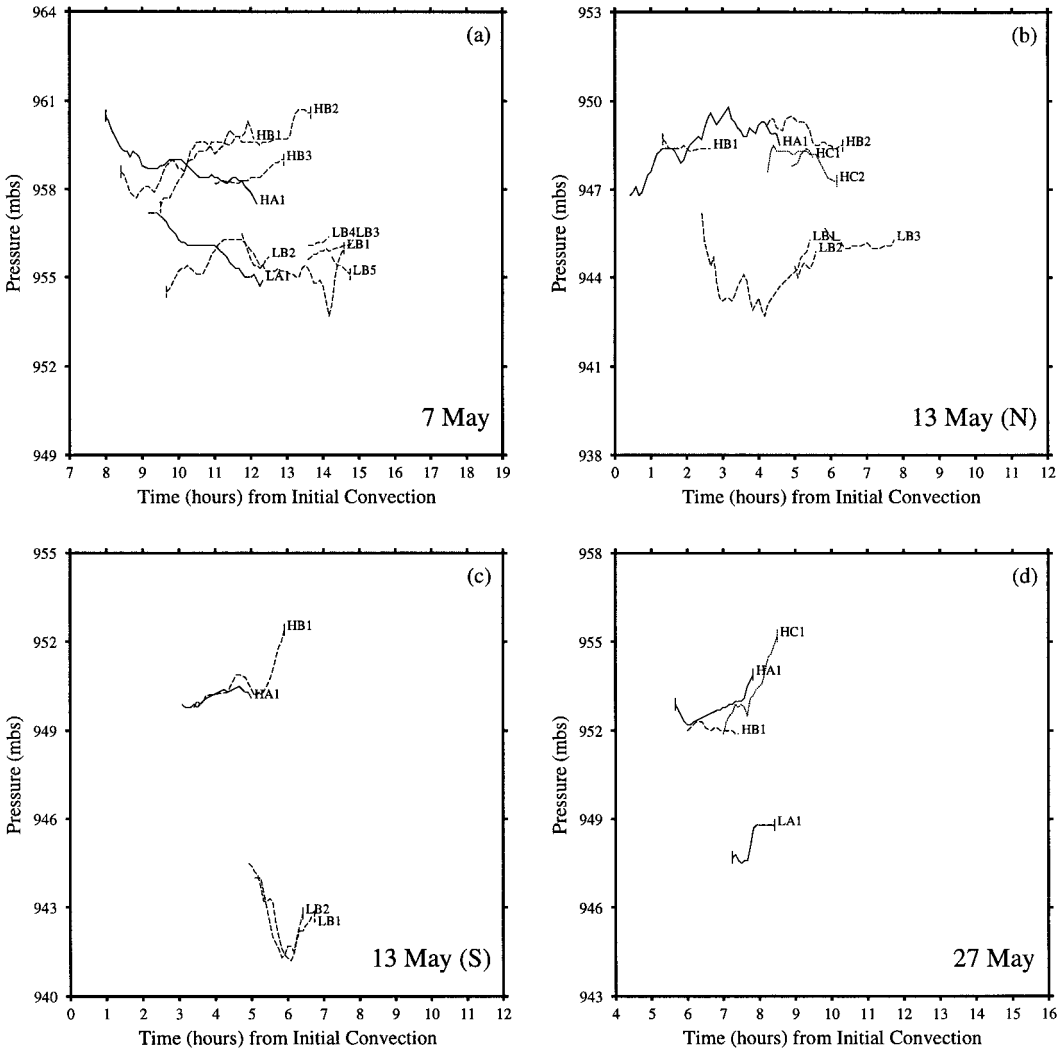

FIG. 9. Central pressures of the transients produced by MCSs on (a) 7 May, (b) 13 May (N), (c) 13 May (S), (d) 27 May, (e) 28 May, (f) 3 June, (g) 3–4 June, (h) 4 June, (i) 10–11 June, (j) 15 June, (k) 24 June, and (l) 26–27 June. On each plot the upper group of traces depicts highs, and the lower depicts lows. A vertical line at the start or end of a trace marks a developed transient's emergence into, or disappearance beyond, the PRE-STORM array.

that the perimeter values are the *total* or *collective* perimeters of the areas influenced by meso-β high and low pressure, not the value of the average transients.

c. Number and perimeter plot similarities

At least two possibilities can explain the extremely close similarity of Figs. 13 and 14. First, the normalization and the area weighting may have introduced into the data a signal strong enough to transform two predominately dissimilar datasets into near duplicates of one another. That is unlikely. Most of the raw, single-MCS plots of transient numbers and collective perimeters (not shown) exhibit the fundamental traits of the composites' plots.

A second possibility is that transients just did not vary greatly in size, either from one to another or from early in one's life to late in one's life. This would mean the most abundant transients produced the greatest collective perimeters, which is precisely what the two figures display. Close inspection of each frame of each movie compels us to side with this second explanation. There were notable exceptions (during the 10–11 June MCS for example) but on the whole, transients did not appear to blossom into vast perturbations late in their lives. In this context, the similarity between Figs. 13 and 14 is further indication that *transitory highs and lows are basic building blocks of mesohighs and wake lows.*

d. Similarity to temporal changes in volumetric rain rates

If transitory highs and lows are products of convective and stratiform kinematics and thermodynamics

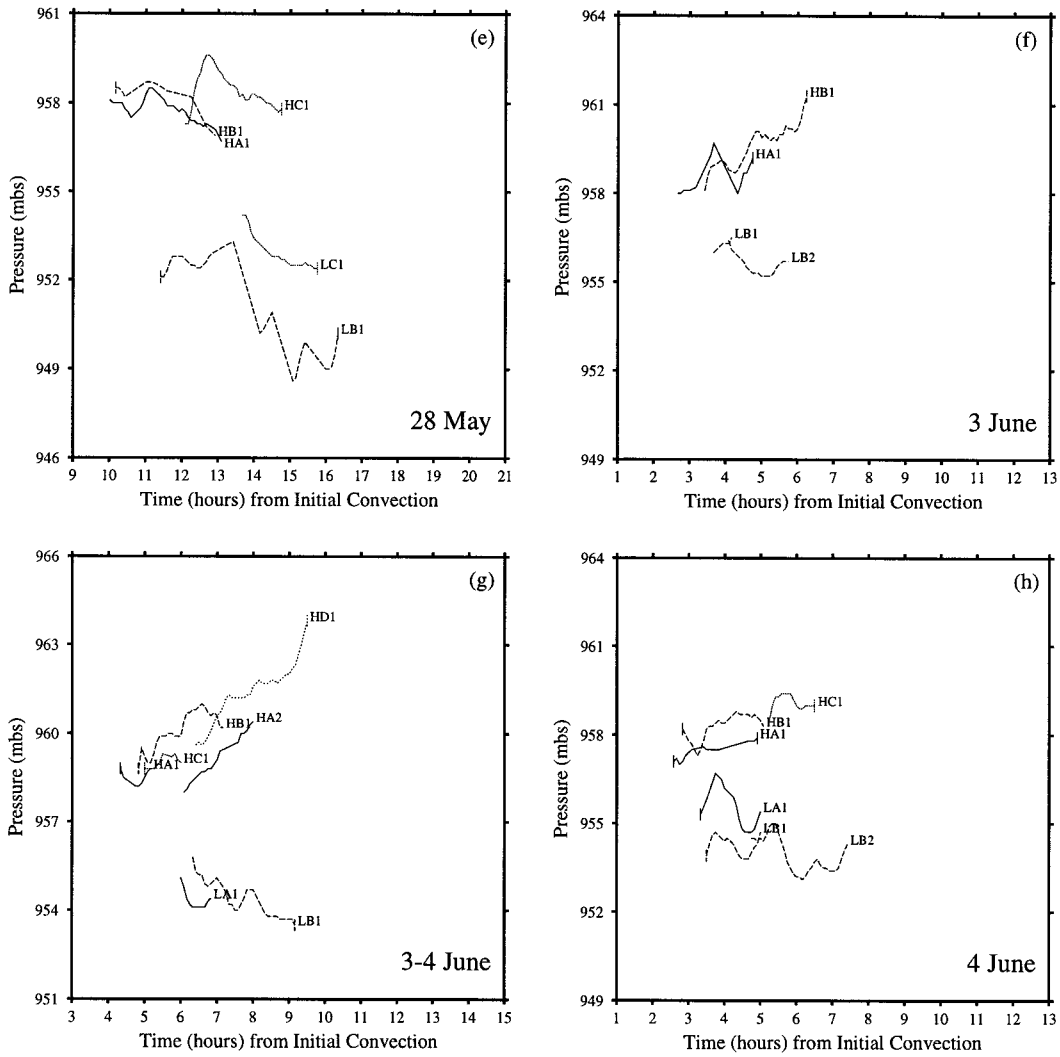

FIG. 9. (*Continued*)

within MCSs, as decades of circumstantial evidence intimate, convective and stratiform rain rates of MCSs should fluctuate in manners that resemble fluctuations of transient numbers and sizes. They do.

McAnelly and Cotton (1992) plotted a composite temporal change in the convective and stratiform rain rates from six MCSs, a few of which were from PRESTORM (Fig. 15). Showers produced increasingly high convective rain rates until just beyond the first third of the composite's life, then the showers' strengths tapered. Steady anvil rain was nearly nonexistent for about 3 h, after which the rate increased, but more slowly than the convective showers. The stratiform rain reached peak intensity about 3 h later than the showers, then slowly weakened. In the last hours of the composite's life, stratiform rain under the anvil fell more heavily than showers at the MCS's leading edge. At their respective maxima, leading-line showers were more intense than the trailing rain.

Differences between McAnelly and Cotton's plot and Figs. 13 and 14 are trivial. The former's β_{MX} and β_{MN} troughs and peaks do not appear in the latter two, but the noise in Fig. 13 and the smoothing in Fig. 14 could be masking them. McAnelly and Cotton's total rain rate peaks later than halfway through the composite's life, but only slightly. Last, the convective rain rate does not vanish to 0 at the end of the composite's life, but the transient numbers and perimeters of Figs. 13 and 14 nearly do.

e. Relevance to theories of upscale evolution

Pedgley (1962) characterized the growth stage of MCSs as a time when ''storms are isolated or in small groups, [then] local pressure rises develop, eventually merging into a thunderstorm high, which then grows in areal extent . . . .'' He added, ''The growth stage is typified by the weather systems becoming progressively more organized.'' Although meteorologists have no

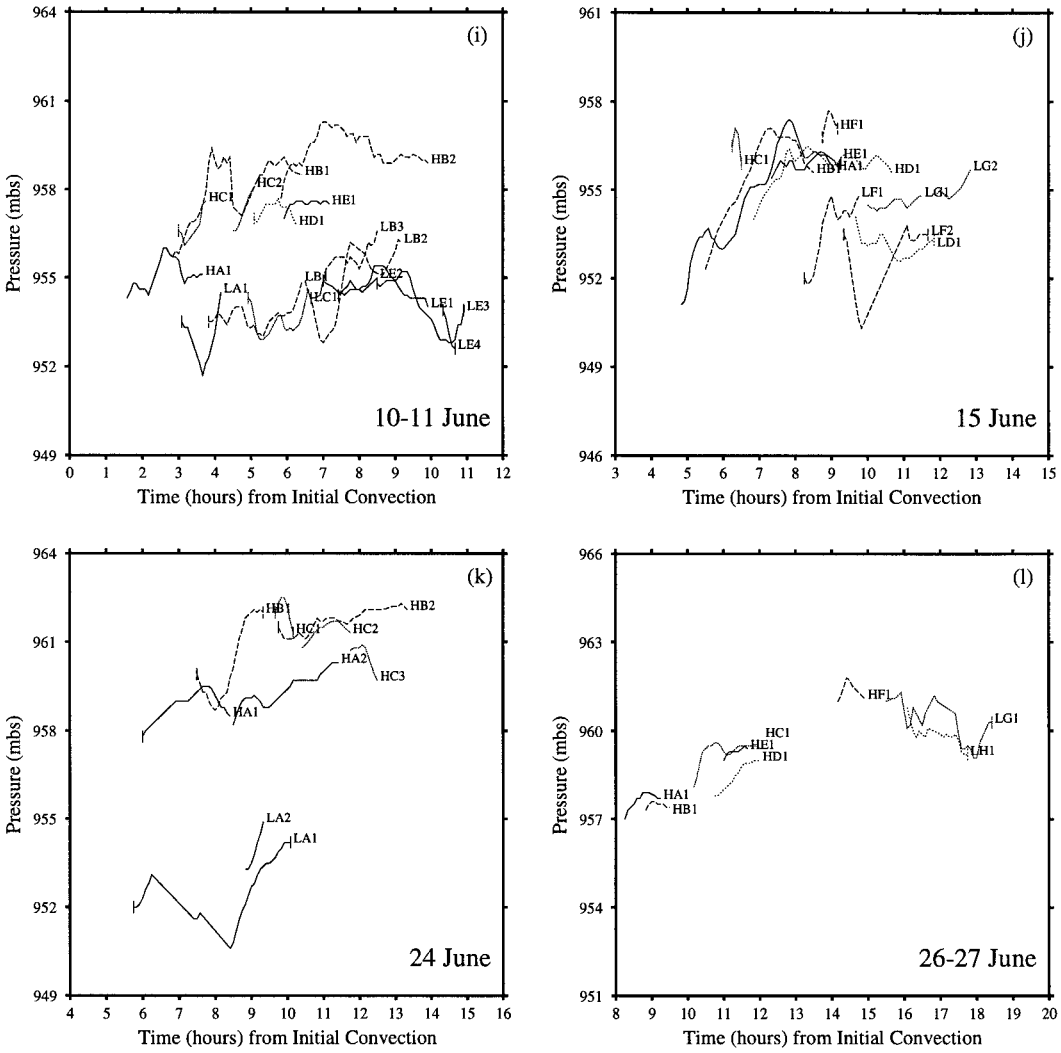

FIG. 9. (*Continued*)

unique and universally accepted definition of upscale evolution, some commonalities include Pedgley's increase in degree of organization and merger of surface pressure features. Additionally, some researchers point to the importance of *sudden growth spurts* that characterize some MCSs' early organizational stages (Nachamkin 1992).

Presumably, during the maturation of the 12 subject MCSs, their meso-β highs and lows should have revealed any such upscale mergers and expansions in two ways: *by becoming fewer and by becoming larger*. They did not—at least not entirely. But there is still room for interpretations of upscale evolution in what *did* happen.

1) TRANSIENT NUMBERS

The curve of the number of transitory highs (Fig. 13) displays a signature consistent with upscale theories (start of trend toward fewer perturbations), while the curve of transitory lows seemingly does not. According to Fig. 13 the merger of convective outflows and consolidation of transitory highs occurred at scaled time 1/3.

The number of transitory lows does not mimic the quick population increase and steady decrease displayed by the highs, perhaps because the formative processes of the former are more complicated. Individual supercells sometimes produce transitory lows, but the cumulonimbi of incipient MCSs are not usually supercells (Rotunno et al. 1988; Houze 1993). It seems a group of ordinary cells must obtain a critical mass, so to speak, before it can noticeably reduce surface pressure rearward of the main convection—a theory that is suggested by Fujita's (1963) diagram of mesosystem pressure cycles (his Fig. 42) and is consistent with modeling by Zhang and Gao (1989). Convective clusters have this critical mass (Nachamkin 1992), so an MCS need not be organized to produce wake lows, but the presence of stratiform rain appears to be critical (Johnson and Hamilton 1988).

Alternatively, the upscale metamorphosis may have occurred just before the first transitory lows appeared, in which case their numbers would not reflect the scale change. In fact, Nachamkin (1992) explains that during the rapid shift in kinematic scales of the 3 June storm, the already-existing mesohigh *intensified* while the wake low *developed* as rear inflow consolidated, strengthened, and descended. The gradual increase in the number of the average transitory lows through most of the remaining observed life may thus have been simply a result of the post-upscale-transition growth of the MCS, because systems do expand for a time after their circulations reach maturity.

Perhaps, too, the convective and stratiform regions of MCSs each undergo their own separately timed upscale growth spurts. Figures 13 and 14 imply the two upscale transitions may be at scaled times 1/3 and 2/3, respectively.

The most likely explanation is the point on which we later elaborate in section 8. Namely, even if many smaller circulations consolidated into a few large meso-α flows, if these few flows impinged on consistently small pockets of high rain or snow rates, the resultant wake lows might have matched the scale of these pockets (Gallus 1996), and so remained at the low end of the meso-β scale, even while the MCS circulations were evolving upscale. In this case, an increase in the number of wake lows, even if they remained small, might also indicate upscale evolution.

2) TRANSIENT PERIMETERS

In Fig. 13, only the increase in transitory highs followed theories of upscale evolution; in Fig. 14 the lows carry the upscale banner. Not until the final quarter of the composite system's observed life, presumably when the MCS's vitality was failing, did the lows' total perimeter begin shrinking. However, the highs' total perimeter decreased steadily from scaled time 1/3. This trend is surprising. The density current character of cumulonimbi cold pools (Wakimoto 1982; Rotunno et al. 1988; Carbone et al. 1990) should theoretically lead to increasingly expansive highs, even while an MCS is in its death throes. Why does this not appear to have happened here?

Transient edges were frustratingly elusive, especially *for the largest transient envelopes.* When cold pools of highs or the dry midtropospheric and surface air of lows apparently expanded so much that transients literally spread themselves too thin to maintain integrity against erosion by fluxes and mixing, we were forced to abandon a vanishing expansive perimeter and redefine a fresher one that closely girded the transient centers. The PAM II and SAM's range, as well as our simple technique, limited how large we could resolve the transients and how long we could track their expansion.

8. Possible transient origins

Most conceptual models of mesohighs and wake lows depict highly elongated perturbations with major axes perpendicular to storm motion. Perturbation aspect ratios from Johnson and Hamilton (1988) exceed 3:1, where the minor axes of both features are roughly 100 km. Other researchers have portrayed mesohighs and wake lows similarly (Fujita 1955; Pedgley 1962; Vescio and Johnson 1992).

In our analyses, instantaneous footprints of transients almost invariably are more circular. But these newly recognized transitory pressure perturbations do not force us to disregard existing theories of mesohigh and wake low origins and search elsewhere for explanations of MCS surface pressure fields.

a. Transitory highs

Squall lines are not uniformly strong along their length. At any one time some of the member cumulonimbi that are arranged shoulder-to-shoulder (Rotunno et al. 1988) are old and some are young; some are weak, others are strong (Fovell and Ogura 1988; Houze et al. 1990). Although their outflows mix, the towers and the convective downdrafts within these towers are separate (Redelsperger and Lafore 1988). Downdraft accelerations and water loading from rain and hail shafts raise surface pressure unequally along the line. But these effects do not wholly explain pronounced pressure variations within mesohighs because 1) pressure changes induced by downdraft momentum and water loading are usually not large enough to account for the entire perturbation high pressure (Bleeker and Andre 1950; Nicholls et al. 1988); and 2) the scale of transitory highs is meso-β, but the instantaneous footprints of the downdraft and rainshaft are convective.

A paper by Fujita (1959) may explain how convective cells within an MCS generate strong and expansive enough thermodynamical forcing to produce transitory highs. Fujita found that a cumulonimbus' evaporatively chilled outflow mass is directly correlated with its rainfall, even though the cold pool spreads beyond the horizontal extent of the main rain shaft (Byers and Braham 1949; Bleeker and Andre 1950). Variable cumulonimbus rainfalls spawn variable cold pool masses that spread from beneath cloud base. In this way, a meso-γ event provokes a meso-β change in boundary layer thermal properties. The increase in integrated atmospheric mass under these cold pools is often sufficient to collectively create a mesohigh (Nicholls et al. 1988).

Cold pools are not born of only chilling liquid drops, however, because above the evaporating rain lies snow that sublimates or melts and also cools the air. Atlas et al. (1969) calculated that melting snow may chill downdrafts 80% as much as evaporating rain. (Of course it is senseless to regard pockets of heavy snow and pockets of heavy rain as two unrelated cold pool mechanisms: the former melt into the latter.) Regardless of what lowers their temperature, mixing and energy fluxes at the edges of neighboring cold pools are insufficient to instantaneously homogenize the entire postsquall boundary layer. Conse-

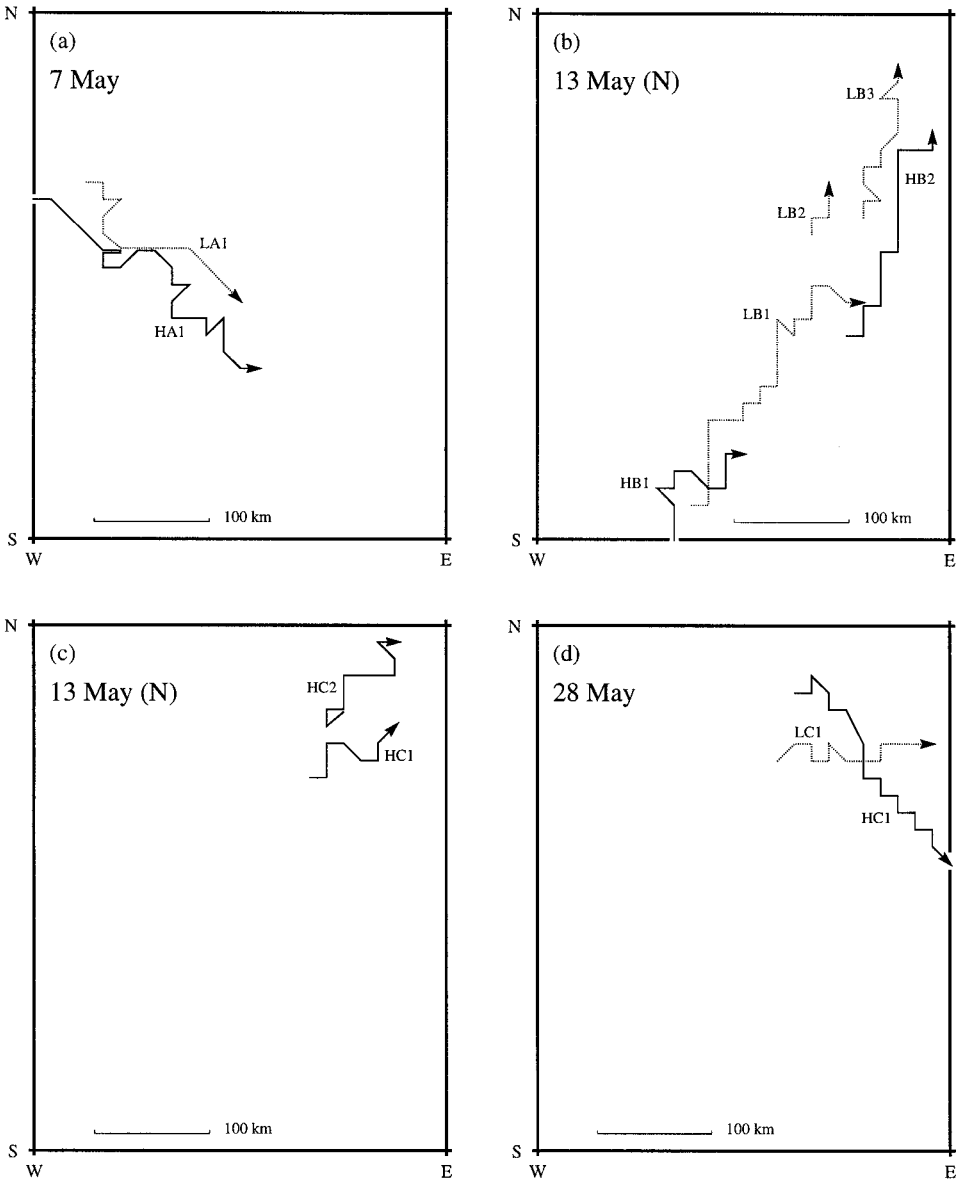

FIG. 10. Paths of transients produced by MCSs on (a) 7 May, (b,c) 13 May (N), (d) 28 May, (e) 3 June, (f) 10–11 June, (g) 15 June, and (h) 24 June.

quently, high pressure strength varies within the overall mesohigh (Williams 1953; Pedgley 1962). These areas of localized higher pressure are high pressure transients. (Recall that we separated the MCS surface pressure transients from the confusing crowd of analyzed meso-β extrema based on transients' collocation with radar reflectivities, thus ensuring that the subject highs and lows were associated with MCS precipitation.)

b. Transitory lows

Many MCS stratiform regions appear to be nearly horizontally homogeneous in infrared or coarse radar imagery, and in their schemata meteorologists often draw anvils as single canopies that overlie broad two-dimensional flows [e.g., Fig. 1 from Houze et al. (1989)]. But stratiform regions apparently harbor vital meso-β inhomogeneities in the rate of latent cooling of the inflow under the anvil (see section 1). These inhomogeneities may produce transitory lows.

The microphysical processes that cool inflow into an MCS are evaporation, sublimation, and melting. On scales internal to the mesoscale cloud system, ''evaporation is the most important latent cooling process determining the structure and strength of the descending rear inflow and the mesoscale downdraft,'' according to Yang and Houze (1995), a conclusion shared by Gallus and Johnson (1995b). Braun and Houze (1997) found

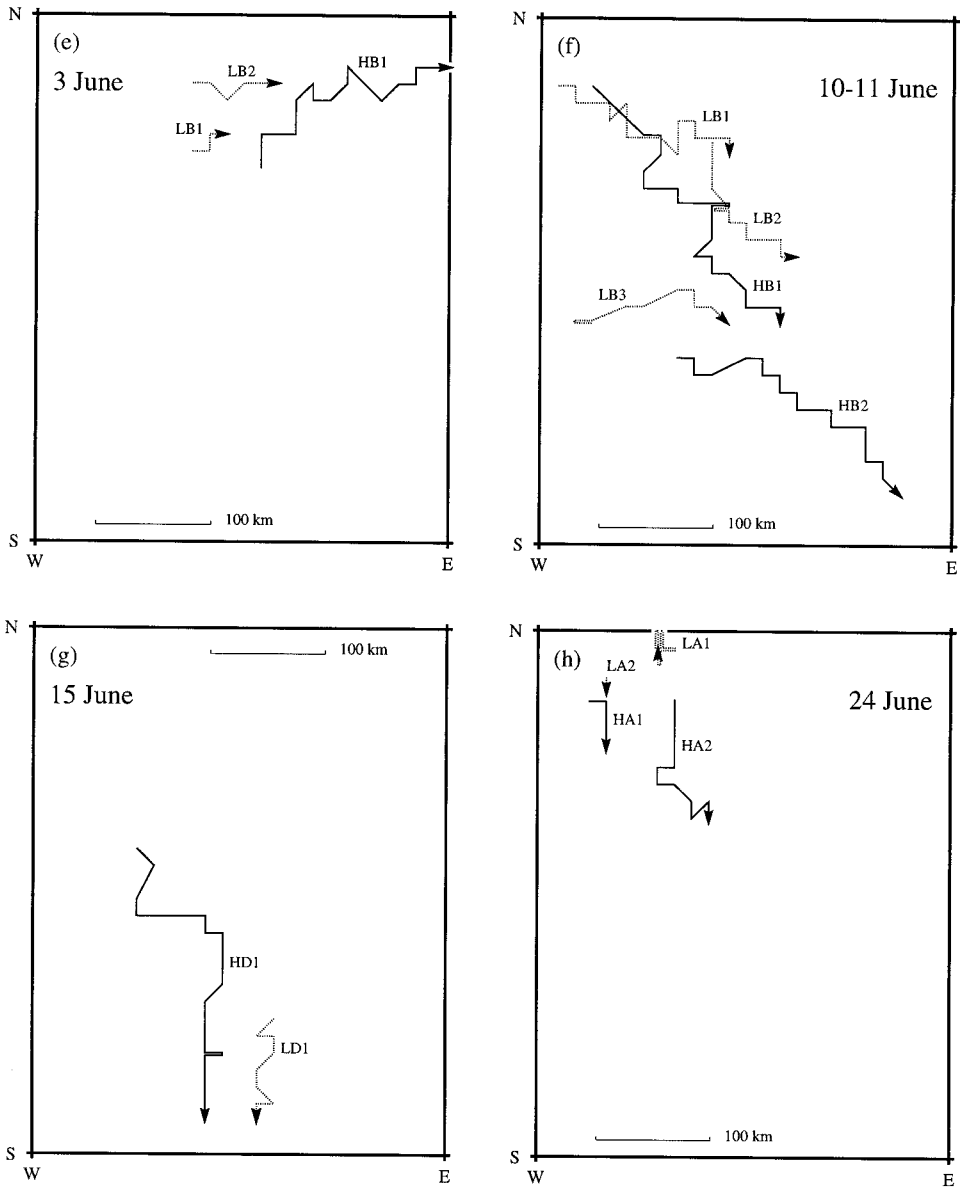

FIG. 10. (*Continued*)

that when they omitted sublimation on the resolvable scale of their nonhydrostatic mesoscale model, the simulated 10–11 June squall line lacked an observed strong core of rear inflow. Additionally, Atlas et al. (1969) and Srivastava (1987) demonstrated the important air-chilling role of melting snow and of other forms of melting ice. Three of the primary factors that determine evaporation, sublimation, and melting in the RTF flow are 1) rain and snow rates, 2) the speed of RTF flow, and 3) the humidity of RTF flow. Inhomogeneities in one or more of these three may be the origins of transitory lows.

1) VARIATIONS IN RAIN AND SNOW RATES

Biggerstaff and Houze (1991) found that meso-β pockets of high rain rates develop in the stratiform region immediately rearward of the most vigorous cells in a convective line. Gallus and Johnson (1995b) agreed. Reflectivities within such pockets of the 10–11 June MCS exceeded those of the lightest stratiform precipitation by up to 20 dB*Z*. Biggerstaff and Houze noted that ''[t]he mesoscale downdraft was most pronounced in the area associated with the strongest precipitation and was, on average, virtually nonexistent in the weak stratiform precipitation region.'' Rutledge et al. (1988) asserted that maxima in sublimative and evaporative cooling actually ''drive'' the mesoscale downdraft.

A multiple Doppler study of a May 1977 squall line over Oklahoma revealed a similar embedded 50-km pocket of 25-dB*Z* stratiform rain (Kessinger et al. 1987). However, the young squall line's stratiform rain was

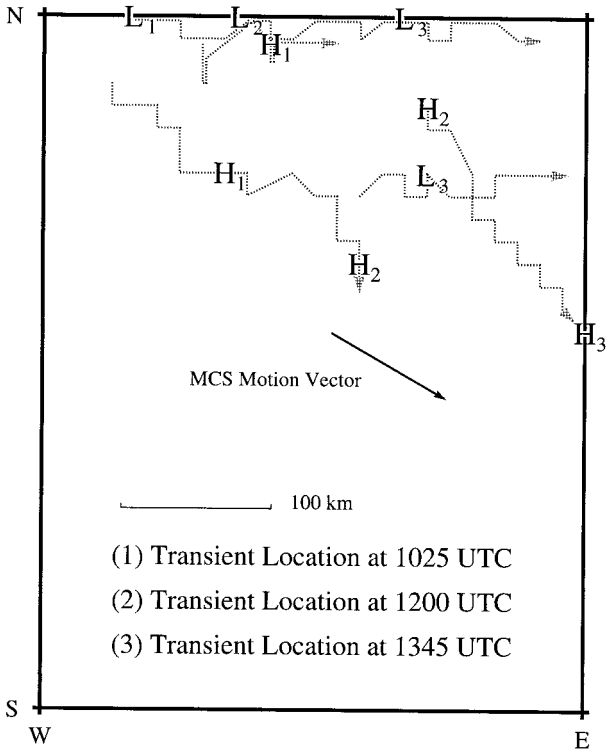

FIG. 11. Skew paths to asymmetry on 28 May 1985. Letters H and L mark, for the times indicated, the locations of the transitory highs and lows named along each path.

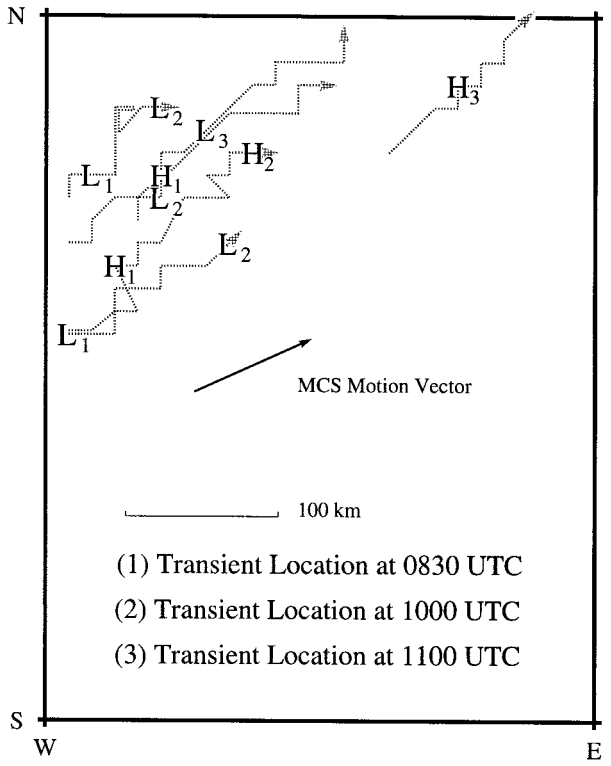

FIG. 12. Parallel paths to asymmetry on 4 June 1985. Letters H and L mark, for the times indicated, the locations of the transitory highs and lows named along each path.

undeveloped, and the RTF flow was weak, so their interactive roles in altering surface pressure is unclear. Zipser (1977), Leary and Rappaport (1987), and Yuter and Houze (1997) found yet other cases of highly inhomogeneous stratiform precipitation.

Generally, immediately above shafts of heavy rain lie shafts of heavy snow, so high rain rates and high snow rates may be categorized together. In one specific study of the distribution of snow mixing ratios within an anvil, Braun and Houze (1997) simulated the 10–11 June MCS with the nonhydrostatic model MM5. Meso-β maxima of snow mixing ratios formed and shortly thereafter invigorated, through sublimative cooling, the proximate part of the modeled RTF flow.

Gallus (1996) implied that horizontal variations in *the change in* precipitation rates may be as successful at generating individual transitory lows within a wake low as horizontal variations in the rates themselves. He found that although invariant snow rates in his two-dimensional cloud model produced high rainfalls and strong subsidence, latent cooling almost negated subsidence warming so no realistically strong wake lows developed. A rapid decrease in the anvil snow rate lessened the latent cooling and generated stronger, more realistic wake lows. Furthermore, in their modeled MCS, Wicker and Skamarock (1996) found that transitory surface lows with gradients of 4 mb km^{-1} formed

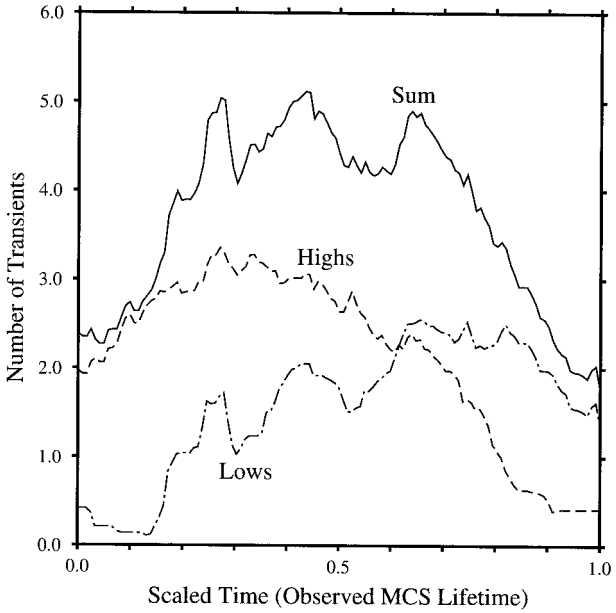

FIG. 13. Composite number of transients vs time. Lines connect data resolved to 5 min. See the appendix for an explanation of the compositing scheme.

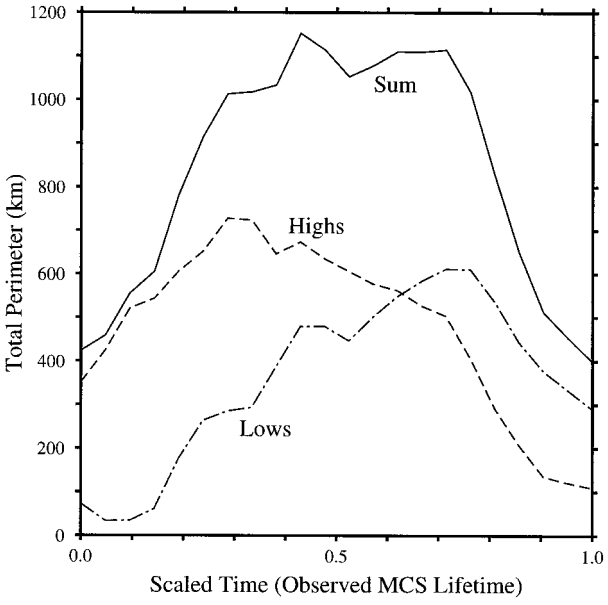

FIG. 14. Composite perimeter of transients vs time. Lines connect data resolved to 30 min. See the appendix for an explanation of the compositing scheme.

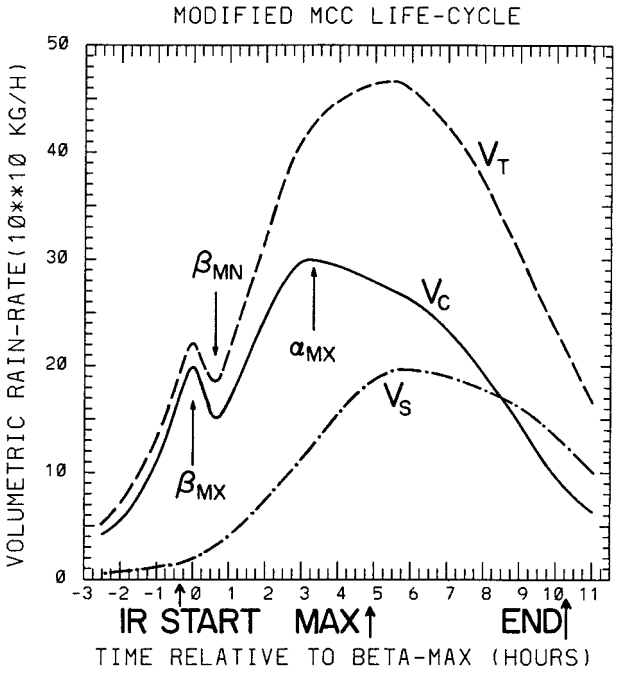

FIG. 15. Composite MCC convective and stratiform volumetric rain rates. Fluctuations in the convective rate V_c and the stratiform rate V_s closely resemble the fluctuations in transient number and size depicted in Figs. 13 and 14. Note that β_{MX} and β_{MN} mark the maximum and minimum in the meso-β-scale cycle of V_c, and α_{MX} marks the maximum in the meso-α-scale cycle of V_c. The total volumetric rain rate is V_t [from McAnelly and Cotton (1992)].

beneath pockets of *collapsing* rain cells upon which strong rear inflow impinged.

For similar reasons, the size of precipitation hydrometeors may be equally as important in determining downdraft strengths. While modeling microbursts, Srivastava (1985, 1987) found that when rainwater mixing ratios were high, smaller rain droplets generated the most intense downdrafts. Smaller droplets are more quickly evaporated away and may produce a thermodynamical effect comparable to that of Gallus' (1996) collapsing precipitation cores.

2) VARIATIONS IN THE SPEED OF REAR-TO-FRONT FLOW

Most studies of RTF flow are two-dimensional. They interpret flow as vast and homogeneous, extending hundreds of kilometers along the back of a squall line and descending uniformly beneath the melting layer. In a study that deviates from this custom, Biggerstaff and Houze (1991) found that flow just below the melting layer in the 10–11 June MCS varied by 2–5 m s^{-1} along the length of the stratiform region. However, the fastest RTF flow was not directly upwind of the deepest surface lows. Their 4-h radar composites were apparently insufficient to display the connection among RTF flow speeds, latent energy exchanges, and rapidly changing surface pressures that is so often buried in microphysical and dynamical complexity (Stumpf et al. 1991; Gallus 1996).

On 28–29 June 1989 a squall line traversed the North Dakota Thunderstorm Project. Klimowski (1994) used five dual-Doppler analyses to monitor the development and character of the line's RTF flow. Flow was broadly strongest behind the northern, most mature part of the line, underneath the most well-developed segment of the anvil. More importantly, local meso-β speed maxima appeared, containing horizontal wind speeds occasionally more than 6 m s^{-1} greater than RTF flow speeds only 20 km away in the along-line direction at the same altitude.

3) VARIATIONS IN THE HUMIDITY OF REAR-TO-FRONT FLOW

Meso-β regions of relatively dry RTF flow may magnify evaporative and sublimative cooling that can lead to more rapid subsidence. Downdrafts that are unsaturated during the latter stages of their descent will, because of horizontal and vertical inertia, overrun their level of neutral buoyancy and warm (Leary 1980; Stensrud et al. 1991; Yang and Houze 1995). Any divergence in response to this warming would reduce the integrated mass in a column of the troposphere and generate a wake low.

Johnson and Hamilton (1988) discovered such dry regions in the RTF flow of the highly scrutinized 10–11 June MCS. Their depictions are composite cross sections compiled from rawinsonde data recorded during 3 h of the MCS's maturity. Relative humidity at a fixed

altitude and distance behind the convective line varied by as much as 30% over 100–200 km. During those 3 h, two strong wake lows existed, separated by a weaker depression. Upwind of both wake lows, RTF flow was relatively strong and dry, whereas in the middle of the stratiform region (measured in distance from both ends), just to the rear of the weak depression, inflow was almost nonexistent and relative humidity surpassed 80% in places. These data imply that weak RTF flow and high humidity in the middle of the squall line hindered the surface depression from deepening to the levels of the lows on the line's ends, where RTF flow was initially drier.

The efficacy of such dryness is apparently limited, however. According to Gallus (1996), as long as the humidity of RTF flow is sufficiently low to foster a certain threshold of net sublimation and evaporation, additional decreases in relative humidity do not significantly deepen wake lows; increases in microphysical cooling offset increases in subsidence warming when precipitation rates are invariant.

Although we have discussed in three separate subsections MCS precipitation rates, RTF flow speeds, and RTF flow humidity, these characteristics likely are interrelated. For instance, speed and humidity may be linked because the higher horizontal momenta in pockets of the fastest RTF flow would favor the most vigorous descent and subsidence drying. We chose three separate discussions simply for reasons of utility. Finally, these kinematical and microphysical arguments are speculative; we do not rule out other explanations.

9. Summary

Animations of time-to-space enhanced surface pressure observations of 12 PRE-STORM MCSs exposed 53 transitory highs and 39 transitory lows that collectively compose spatial and temporal envelopes that contribute at least part of the total pressure field within mesohighs and wake lows. Transitory highs are possibly products of varied hydrometeor loads, varied downdraft strengths, and varied latent cooling magnitudes among MCSs' leading cumulonimbi. Transitory lows are possibly products of horizontal meso-β inhomogeneities in stratiform precipitation rate, RTF flow speed, and RTF flow humidity.

In the 12 subject MCSs most transitory highs existed detectably less than 1.5 h, but some persisted for more than 4 h. Their average sampled lifetime was 124 min. Most transitory lows also existed detectably less than 1.5 h. The most persistent lows were detectable for more than 3 h, and the average transitory low's sampled lifetime was 91 min. Transitory high sampled displacements ranged roughly from 0 to 350 km and averaged 115 km, but most highs traveled a net detectable distance of less than 150 km. Even the most well-traveled transitory lows had detectable displacements of 250 km or less. Transitory low detectable displacements averaged 84 km, and most lows traveled a net detectable distance of roughly 50 km. We could not reliably measure transients' sizes because their perimeters were often hard to locate, but they apparently had horizontal dimensions of roughly 100 km (approximately twice the surface station spacing). Transients did not apparently favor formation or dissipation in any location of the pressure envelopes.

A quasi-Lagrangian analysis of strengths of the 92 transients produced traces that bore four primary signatures: 1) synoptic and storm-scale, 2) the relative forcing by the convective lines and stratiform areas, 3) trends within families of closely associated highs and lows, and 4) fluctuations of each unique transient. At the first scale, the pressure rose in five (42%) cases, fell in one (8%) case, and did not change significantly in three (25%) cases; three (25%) cases are inconclusive. On the second scale, 7 of 12 (58%) MCSs exhibit diffluent high and low pressure trends (that is, the central pressures of transitory highs increased while the central pressures of transitory lows decreased), two (17%) MCSs' trends are nondiffluent, and three (25%) are inconclusive. On the third scale, there is no conclusive evidence that transitory highs consistently strengthened before transitory lows within the same family, although envelopes of high pressure did generally strengthen before envelopes of low pressure. Finally, no systematic patterns appeared in the fourth and finest scale. Transient magnitudes were a few millibars.

Transient paths reflect MCSs' occasional asymmetrization (Houze et al. 1990; Skamarock et al. 1994; Loehrer and Johnson 1995). Most paths were hybrids of two intra-MCS patterns: skew and parallel. Both patterns were vehicles for asymmetrical rearrangements of transients that were initially symmetrically or quasi-symmetrically arranged. In the skew cases, transients' confluent or diffluent paths shifted them toward increasingly asymmetric relative positions. In the parallel cases, initial transients were replaced by transients that formed in increasingly asymmetrically arranged locations.

Temporal changes in the numbers and sizes of the transients produced by a composite MCS partially support and partially refute theories of upscale evolution, but the refutations are probably a product of problems within the compositing scheme and of the frequently difficult detection of aged transient perimeters. The number of transitory highs increased sharply through the first third of the composite's life, then slowly decreased, presumably as the outflows from various convective cells merged, which supports upscale evolution theories. The number of transitory lows began increasing later and increased more slowly through two-thirds of the composite's life before decreasing late, which does not support upscale evolution theories founded on simultaneous consolidations of convective and stratiform flows near the start of MCSs' maturity. But examining transients' sizes was difficult and subjective because perimeters disappeared from the plots as tran-

sients' modified air expanded and surface fluxes and mixing eroded their perimeter gradients, so we were biased toward excluding transients at their largest and oldest.

Temporal changes in the numbers and sizes of the composite's transients closely resemble fluctuations in the composite MCS volumetric rain rates of McAnelly and Cotton (1992). The similarities complement the already persuasive wealth of circumstantial evidence associating MCS mesohighs and wake lows with convective and stratiform precipitation, respectively.

10. Conclusions

Perhaps meteorologists have not widely scrutinized pressure transients, especially in the contexts of MCS microphysics and precipitation, because 1) most station pressure data are spatially too coarse to resolve the divisions between one transient and its neighbor, 2) some data are temporally too coarse to mark the dissipation of one transient and the formation of another, and 3) on single, unanimated plots of station pressure, transients are indistinguishable from noise and instrument errors. *Only the fluid, continuous variations in the pressure field from one movie frame to the next differentiate signatures of real meso-β transients from artifacts within the data.* We cannot overemphasize this.

Transients within mesohighs and wake lows should not surprise us. Moreover, transients themselves likely harbor another set of yet smaller, more fleeting perturbations, and probably within those exist more highs and lows, and so on. Such is the nature of a perturbed fluid with low viscosity.

The 92 detected transients likely owe some of their size to the observing array resolution, but we are confident that the transients are not *entirely* an artifact of the scientific system used to detect them. The atmosphere is nondiscrete for all meteorologists' attempts at discretization, but much of the atmosphere's energy does reside at preferred temporal and spatial scales (convective updrafts are about 1–5 km across, for instance). In the case of MCS transients, *finding such preferred scales is a critical part of the search for the origins of postsquall MCS surface pressure perturbations.* Evidence for what produces mesohighs, wake lows, and the transients within them is so far primarily circumstantial; meteorologists note collocations and associations, and they find phenomena that could theoretically increase or reduce the surface pressure by the amount observed. But the proposed mechanisms must explain not only the magnitude of the perturbed pressure, but also the *temporal and spatial scales of the perturbations,* which we cannot know without more detailed fieldwork.

Are individual transitory highs and transitory lows uniquely linked to one another, or do links exist only at the envelope scale and not at the finer end of the spectrum? For utilitarian reasons we inferred in this paper loose physical associations, but often on sketchy evidence. We have not proven that the two classes of transients are dynamically linked, but the conclusions herein do not require a link.

Evidence that mesohighs and wake lows harbor transients should not be confused with an argument that transients produce the entire pressure perturbation within mesohighs and wake lows. Recent papers such as Pandya and Durran (1996) make it seem likely that gravity waves, and perhaps other phenomena, share with transients the responsibility for the meso-β pressure perturbations observed beneath MCSs.

Acknowledgments. The National Science Foundation supported our research under Grant ATM-9313716. Scot Loehrer supplied PRE-STORM surface and radar data, and we based some of our analyses on his techniques. Paul Ciesielski, Patrick Haertel, Eric Hilgendorf, Xin Lin, and Rick Taft rescued us from many computing misfortunes. Gerald Callahan, Michael Fortune, Robert Houze Jr., Ray McAnelly, Thomas McKee, and Jason Nachamkin commented insightfully on our work and suggested fruitful research paths. Gail Cordova helped us typeset our submitted manuscript. We animated our data with the NCAR graphics 3.2 X-Window Interactive Display Tool (IDT).

APPENDIX

Creation of MCS Composite

The longest interval during which pressure transients from any single MCS were observed within the PRE-STORM array is 10 h 10 min for the 26–27 June storm. To prepare all the systems' data for a composite, we matched the observed beginning, midpoint, and end of all 12 events by 1) separating by 10 h 10 min the beginning and end of the other 11 storms, then 2) interpolating each station's raw data to the expanded interval.

We normalized pressure data from the convective and stratiform regions to compensate for incomplete areal sampling of MCSs partially beyond the perimeter of the PRE-STORM array. The process involves dividing the number of recorded transients or the perimeter of recorded transients by the sampled fraction of pertinent MCS region, stratiform for lows and convective for highs. Using plots of radar reflectivity we determined the sampled fractions of the MCSs only to the nearest 20%, beginning at 20% (in order to avoid an infinite correction factor), and each 5-min plot received its own two correction factors (Fig. 13). For example, if the PRE-STORM network detected three transitory highs beneath an MCS's convective line, and only 40% of the line fell within the array, we normalized the three transients to seven and a half transients.

The area normalization's validity rests on the assumption that transients are distributed uniformly within their spawning zones. For any one MCS at any one time the assumption is invalid, but the composite encom-

passes 12 MCSs and 855 total observations. The large sample averaged unsystematic inaccuracies in the assumption and produced a reasonable composite representation.

For the second composite (Fig. 14), we resolved the plot to 30 min instead of 5 min, which explains the apparent smoothing. The data themselves are not truly size data—they are values of perimeter, not area. However, in most cases transients were quasi-circular so areas roughly correspond to the square of perimeters divided by 4π.

When transients abutted one another to create one envelope of perturbed surface pressure, we traced only the perimeter of the envelope; rarely could we tell where one transient ended and another began in such cases. As an unwanted side effect, multiple transients that were close but not touching one moment might barely merge in the next plot and produce a sharp, artificial decrease in perimeter. The outer edge of the highest local pressure gradient usually marked an envelope perimeter. When it did not, we subjectively defined the edge based on an assumption of quasi-circularity or by interpolating between earlier and later plots that did display distinct edges. In Fig. 14 the perimeters have units, but we only have confidence in the relative values, not in the exact measurements.

REFERENCES

Atlas, D., R. Tatehira, R. C. Srivastava, W. Marker, and R. E. Carbone, 1969: Precipitation-induced mesoscale wind perturbations in the melting layer. *Quart. J. Roy. Meteor. Soc.,* **95,** 544–560.

Barnes, S. L., 1964: A technique for maximizing details in numerical weather map analysis. *J. Appl. Meteor.,* **3,** 396–409.

Biggerstaff, M. I., and R. A. Houze Jr., 1991: Kinematic and precipitation structure of the 10–11 June 1985 squall line. *Mon. Wea. Rev.,* **119,** 3034–3065.

Bleeker, W., and M. J. Andre, 1950: Convective phenomena in the atmosphere. *J. Meteor.,* **7,** 195–209.

Bluestein, H. B., 1992: *Synoptic–Dynamic Meteorology in Midlatitudes.* Vol. 1, *Principles of Kinematics and Dynamics,* Oxford University Press, 431 pp.

Bosart, L. F., and J. P. Cussen Jr., 1973: Gravity wave phenomena accompanying east coast cyclogenesis. *Mon. Wea. Rev.,* **101,** 446–454.

Braham, R. R., 1952: The water and energy budgets of the thunderstorm and their relation to thunderstorm development. *J. Meteor.,* **9,** 227–242.

Braun, S. A., and R. A. Houze Jr., 1994: The transition zone and secondary maximum of radar reflectivity behind a midlatitude squall line: Results retrieved from Doppler radar data. *J. Atmos. Sci.,* **51,** 2733–2755.

——, and ——, 1997: The evolution of the 10–11 June PRE-STORM squall line: Initiation, development of rear inflow, and dissipation. *Mon. Wea. Rev.,* **125,** 478–504.

Brown, H. A., 1963: On the low-level structure of a squall line. Mesometeorology Research Paper 21, Dept. of Geophysical Sciences, University of Chicago, Chicago, IL, 19 pp. [Available from Dept. of Geophysical Sciences, University of Chicago, 5734 S. Ellis Ave., Chicago, IL 60637.]

Brunk, I. W., 1949: The pressure pulsation of 11 April 1944. *J. Meteor.,* **6,** 181–187.

——, 1953: Squall lines. *Bull. Amer. Meteor. Soc.,* **34,** 1–9.

Byers, H. R., and R. R. Braham, 1949: *The Thunderstorm.* U.S. Weather Bureau, U.S. Department of Commerce, Washington, DC, 287 pp.

Carbone, R. E., J. W. Conway, N. A. Crook, and M. W. Moncrieff, 1990: The generation and propagation of a nocturnal squall line. Part I: Observations and implications for mesoscale predictability. *Mon. Wea. Rev.,* **118,** 26–49.

Chapman, S., and R. S. Lindzen, 1970: *Atmospheric Tides.* Reidel, 200 pp.

Chong, M., P. Amayenc, G. Scialom, and J. Testud, 1987: A tropical squall line observed during the COPT 81 experiment in West Africa. Part I: Kinematic structure inferred from dual-Doppler radar data. *Mon. Wea. Rev.,* **115,** 670–694.

Cunning, J. B., 1986: The Oklahoma–Kansas Preliminary Regional Experiment for STORM-Central. *Bull. Amer. Meteor. Soc.,* **67,** 1478–1486.

Fovell, R. G., and Y. Ogura, 1988: Numerical simulation of a midlatitude squall line in two dimensions. *J. Atmos. Sci.,* **45,** 3846–3879.

Fujita, T. T., 1955: Results of detailed synoptic studies of squall lines. *Tellus,* **7,** 405–436.

——, 1959: Precipitation and cold air production in mesoscale thunderstorm systems. *J. Meteor.,* **16,** 454–466.

——, 1963: Analytical mesometeorology: A review. *Severe Local Storms, Meteor. Monogr.,* No. 27, Amer. Meteor. Soc., 77–125.

——, 1985: The downburst: Microburst and macroburst. SMRP Research Paper 210, Dept. of Geophysical Sciences, University of Chicago, Chicago, IL, 122 pp. [NTIS PB-148880.]

Gallus, W. A., Jr., 1996: The influence of microphysics in the formation of intense wake lows: A numerical modeling study. *Mon. Wea. Rev.,* **124,** 2267–2281.

——, and R. H. Johnson, 1995a: The dynamics of circulations within the trailing stratiform regions of squall lines. Part I: The 10–11 June PRE-STORM System. *J. Atmos. Sci.,* **52,** 2161–2187.

——, 1995b: The dynamics of circulations within the trailing stratiform regions of squall lines. Part II: Influence of the convective line and ambient environment. *J. Atmos. Sci.,* **52,** 2188–2211.

Heymsfield, G. M., and S. Schotz, 1985: Structure and evolution of a severe squall line over Oklahoma. *Mon. Wea. Rev.,* **113,** 1563–1589.

Houze, R. A., Jr., 1993: *Cloud Dynamics.* Academic Press, 573 pp.

——, and E. N. Rappaport, 1984: Air motions and precipitation structure of an early summer squall line over the eastern tropical Atlantic. *J. Atmos. Sci.,* **41,** 553–574.

——, B. F. Smull, and P. Dodge, 1990: Mesoscale organization of springtime rainstorms in Oklahoma. *Mon. Wea. Rev.,* **118,** 613–654.

Humphreys, W. J., 1929: *The Physics of the Air.* McGraw-Hill, 654 pp.

Johnson, R. H., and J. J. Toth, 1986: Preliminary data quality analysis for May–June 1985 Oklahoma-Kansas PRE-STORM PAM-II mesonetwork. Atmospheric Science Paper 407, Dept. of Atmospheric Science, Colorado State University, Fort Collins, CO, 41 pp. [Available from Dept. of Atmospheric Science, Colorado State University, Fort Collins, CO 80523-1371.]

——, and P. J. Hamilton, 1988: The relationship of surface pressure features to the precipitation and airflow structure of an intense midlatitude squall line. *Mon. Wea. Rev.,* **116,** 1444–1472.

Kessinger, C. J., P. S. Ray, and C. E. Hane, 1987: The 19 May 1977 Oklahoma squall line. Part I: A multiple Doppler analysis of convective and stratiform structure. *J. Atmos. Sci.,* **44,** 2840–2864.

Klimowski, B. A., 1994: Initiation and development of rear inflow within the 28–29 June 1989 North Dakota mesoconvective system. *Mon. Wea. Rev.,* **122,** 765–779.

Koch, S. E., P. B. Dorian, and R. E. Golos, 1988: A mesoscale gravity wave event observed during CCOPE. Part I: Multiscale statistical analysis of wave characteristics. *Mon. Wea. Rev.,* **116,** 2527–2544.

Krumm, W. R., 1954: On the cause of downdrafts from dry thun-

derstorms over the plateau area of the United States. *Bull. Amer. Meteor. Soc.,* **35,** 122–125.

Leary, C. A., 1980: Temperature and humidity profiles in mesoscale unsaturated downdrafts. *J. Atmos. Sci.,* **37,** 1005–1012.

——, and E. N. Rappaport, 1987: The life cycle and internal structure of a mesoscale convective complex. *Mon. Wea. Rev.,* **115,** 1503–1527.

Ligda, M. G. H., 1956: The radar observation of mature pre-frontal squall lines in the midwestern United States. *Contrib. Oceanogr. Meteor.,* **3** (60–89), 153–155.

Loehrer, S. M., 1992: The surface pressure features and precipitation structure of PRE-STORM mesoscale convective systems. Atmospheric Science Paper 518, Dept. of Atmospheric Science, Colorado State University, Fort Collins, CO, 296 pp. [Available from Dept. of Atmospheric Science, Colorado State University, Fort Collins, CO 80523-1371.]

——, and R. H. Johnson, 1995: Surface pressure and precipitation life cycle characteristics of PRE-STORM mesoscale convective systems. *Mon. Wea. Rev.,* **123,** 600–621.

McAnelly, R. L., and W. R. Cotton, 1992: Early growth of mesoscale convective complexes: A meso-β-scale cycle of convective precipitation? *Mon. Wea. Rev.,* **120,** 1851–1877.

Nachamkin, J. E., 1992: The upscale evolution of a midlatitude mesoscale convective complex. Atmospheric Science Paper 498, Dept. of Atmospheric Science, Colorado State University, Fort Collins, CO, 122 pp. [Available from Dept. of Atmospheric Science, Colorado State University, Fort Collins, CO 80523-1371.]

Newton, C. W., 1950: Structure and mechanism of the pre-frontal squall line. *J. Meteor.,* **7,** 210–222.

——, 1966: Circulations in large sheared cumulonimbus [sic]. *Tellus,* **18,** 699–712.

——, and J. C. Fankhauser, 1964: On the movements of convective storms, with emphasis on size distribution in relation to water-budget requirements. *J. Appl. Meteor.,* **3,** 651–668.

Nicholls, M. E., R. H. Johnson, and W. R. Cotton, 1988: The sensitivity of two-dimensional simulations of tropical squall lines to environmental profiles. *J. Atmos. Sci.,* **45,** 3625–3649.

Ogura, Y., and M. T. Liou, 1980: The structure of the midlatitude squall line: A case study. *J. Atmos. Sci.,* **37,** 553–567.

Orlanski, I., 1975: A rational subdivision of scales for atmospheric processes. *Bull. Amer. Meteor. Soc.,* **56,** 527–530.

Pandya, R. E., and D. R. Durran, 1996: The influence of convectively generated thermal forcing on the mesoscale circulation around squall lines. *J. Atmos. Sci.,* **53,** 2924–2951.

Pedgley, D. E., 1962: A meso-synoptic analysis of the thunderstorms on 28 August 1958. U.K. Meteor. Office Geophys. Memo. 106, 74 pp. [Available from U.K. Meteorological Office, Room 709, London Road, Bracknell, Berkshire RG12 2SZ, United Kingdom.]

Redelsperger, J.-L., and J.-P. Lafore, 1988: A three-dimensional simulation of a tropical squall line: Convective organization and thermodynamic transport. *J. Atmos. Sci.,* **45,** 1334–1356.

Riehl, H., 1968: Some aspects of cumulus-scale downdrafts. Atmospheric Science Paper 126, Part 1, Dept. of Atmospheric Science, Colorado State University, Fort Collins, CO, 32 pp. [Available from Dept. of Atmospheric Science, Colorado State University, Fort Collins, CO 80523-1371.]

Rotunno, R., J. B. Klemp, and M. L. Weisman, 1988: A theory for strong, long-lived squall lines. *J. Atmos. Sci.,* **45,** 463–485.

Roux, F., 1988: The West African squall line observed on 23 June 1981 during COPT 81: Kinematics and thermodynamics of the convective region. *J. Atmos. Sci.,* **45,** 406–426.

Rutledge, S. A., R. A. Houze Jr., M. I. Biggerstaff, and T. Matejka, 1988: The Oklahoma-Kansas mesoscale convective system of 10–11 June 1985: Precipitation structure and single-Doppler radar analysis. *Mon. Wea. Rev.,* **116,** 1409–1430.

Sanders, F., and K. A. Emanuel, 1977: The momentum budget and temporal evolution of a mesoscale convective system. *J. Atmos. Sci.,* **34,** 322–330.

Sawyer, J. S., 1946: Cooling by rain as the cause of the pressure rise in convective squalls. *Quart. J. Roy. Meteor. Soc.,* **72,** 168.

Schmidt, J. M., and W. R. Cotton, 1989: A High Plains squall line associated with severe surface winds. *J. Atmos. Sci.,* **46,** 281–302.

Schubert, W. H., J. J. Hack, P. L. Silva Dias, and S. R. Fulton, 1980: Geostrophic adjustment in an axisymmetric vortex. *J. Atmos. Sci.,* **37,** 1464–1484.

Scott, J. D., and S. A. Rutledge, 1995: Doppler radar observations of an asymmetric MCS and associated vortex couplet. *Mon. Wea. Rev.,* **123,** 3437–3457.

Shaw, W. N., and W. H. Dines, 1905: The study of the minor fluctuations of atmospheric pressure. *Quart. J. Roy. Meteor. Soc.,* **31,** 39–52.

Skamarock, W. C., M. L. Weisman, and J. B. Klemp, 1994: Three-dimensional evolution of simulated long-lived squall lines. *J. Atmos. Sci.,* **51,** 2563–2584.

Smull, B. F., and R. A. Houze Jr., 1987a: Dual-Doppler radar analysis of a midlatitude squall line with a trailing region of stratiform rain. *J. Atmos. Sci.,* **44,** 2128–2148.

——, and ——, 1987b: Rear inflow in squall lines with trailing stratiform precipitation. *Mon. Wea. Rev.,* **115,** 2869–2889.

Sommeria, G., and J. Testud, 1984: COPT 81: A field experiment designed for the study of dynamics and electrical activity of deep convection in continental tropical regions. *Bull. Amer. Meteor. Soc.,* **65,** 4–10.

Srivastava, R. C., 1985: A simple model of evaporatively driven downdraft: Application to microburst downdraft. *J. Atmos. Sci.,* **42,** 1004–1023.

——, 1987: A model of intense downdrafts driven by the melting and evaporation of precipitation. *J. Atmos. Sci.,* **44,** 1752–1773.

——, T. J. Matejka, and T. J. Lorello, 1986: Doppler radar study of the trailing anvil region associated with a squall line. *J. Atmos. Sci.,* **43,** 356–377.

Stensrud, D. J., R. A. Maddox, and C. L. Ziegler, 1991: A sublimation-initiated mesoscale downdraft and its relation to the wind field below a precipitating anvil cloud. *Mon. Wea. Rev.,* **119,** 2124–2139.

Stumpf, G. J., 1988: Surface pressure features associated with a mesoscale convective system in O.-K. PRE-STORM. Atmospheric Science Paper 435, Dept. of Atmospheric Science, Colorado State University, Fort Collins, CO, 148 pp. [Available from Dept. of Atmospheric Science, Colorado State University, Fort Collins, CO 80523-1371.]

——, R. H. Johnson, and B. F. Smull, 1991: The wake low in a midlatitude mesoscale convective system having complex convective organization. *Mon. Wea. Rev.,* **119,** 134–158.

Suckstorff, G. A., 1935: Die Strömungsvorgänge in Instabilitätsschauern. *Z. Meteor.,* **25,** 449–452.

——, 1939: Die Ergebnisse der Untersuchungen an tropischen Gewittern und einigen anderen Erscheinungen. *Gerlands Beitr. Geophysik,* **55,** 138–185.

Vescio, M. D., and R. H. Johnson, 1992: The surface-wind response to transient mesoscale pressure fields associated with squall lines. *Mon. Wea. Rev.,* **120,** 1837–1850.

Wakimoto, R. M., 1982: The life cycle of thunderstorm gust fronts viewed with Doppler radar and rawinsonde data. *Mon. Wea. Rev.,* **110,** 1060–1082.

Wicker, L. J., and W. C. Skamarock, 1996: The dynamics governing surface pressure fields in mesoscale convective systems. Preprints, *Seventh Conf. on Mesoscale Processes,* Reading, United Kingdom, Amer. Meteor. Soc., 476–478.

Williams, D. T., 1948: A surface micro-study of squall-line thunderstorms. *Mon. Wea. Rev.,* **76,** 239–246.

——, 1953: Pressure wave observations in the central Midwest, 1952. *Mon. Wea. Rev.,* **81,** 278–289.

——, 1963: The thunderstorm wake of May 4, 1961. National Severe Storms Project Rep. 18, U.S. Dept. of Commerce, Washington, DC, 23 pp. [NTIS PB-168223.]

Yang, M.-J., and R. A. Houze Jr., 1995: Sensitivity of squall-line rear inflow to ice microphysics and environmental humidity. *Mon. Wea. Rev.,* **123,** 3175–3192.

——, and ——, 1996: Momentum budget of a squall line with trailing stratiform precipitation: Calculations with a high-resolution numerical model. *J. Atmos. Sci.,* **53,** 3629–3652.

Yuter, S. E., and R. A. Houze Jr., 1997: Measurements of raindrop size distributions over the Pacific warm pool and implications for *Z–R* relations. *J. Appl. Meteor.,* **36,** 847–867.

Zhang, D.-L., and K. Gao, 1989: Numerical simulation of an intense squall line during 10–11 June 1985 PRE-STORM. Part II: Rear inflow, surface pressure perturbations, and stratiform precipitation. *Mon. Wea. Rev.,* **117,** 2067–2094.

Zipser E. J., 1969: The role of organized unsaturated convective downdrafts in the structure and rapid decay of an equatorial disturbance. *J. Appl. Meteor.,* **8,** 799–814.

——, 1977: Mesoscale and convective scale downdrafts as distinct components of squall-line structure. *Mon. Wea. Rev.,* **105,** 1568–1589.